SE-CNN-BiLSTM Lithium-ion Battery SOC Prediction Model Based on Bayesian Optimization and Wavelet Denoising

Song-Bo Zhang, Jie-Sheng Wang*, Chun-Ni Shi, Xiao-Tian Wang, Jun-Yu Lu

Abstract—**Precise estimation of the State of Charge (SOC) is crucial for ensuring the safety and optimizing the performance of lithium-ion batteries in electric vehicles and energy storage systems. A SE-CNN-BiLSTM SOC prediction model that integrates Bayesian optimization and wavelet denoising techniques was proposed. Initially, the original dataset undergoes wavelet transform for denoising, effectively mitigating noise interference while preserving critical signal features. Subsequently, a convolutional neural network (CNN) augmented with a Squeeze-and-Excitation (SE) module is employed to extract features from the denoised data, thereby improving the model's capacity to assign varying weights to different features and enhancing feature representation efficacy. Building upon this foundation, Bayesian optimization is applied to fine-tune parameters such as neuron count, learning rate and L2 regularization coefficient within the bidirectional long short-term memory network (BiLSTM), ensuring robust prediction accuracy and generalization capabilities in complex dynamic environments. Finally, these extracted features are fed into the optimized BiLSTM for SOC forecasting. The experimental data and simulation analyses are derived from the Turnigy Graphene 5000mAh 65C lithium-ion battery, validated under three distinct temperature conditions: -10℃, 0℃, and 10℃. The findings indicate that the proposed model excels in state of charge (SOC) prediction, achieving not only superior accuracy compared to traditional methodologies but also demonstrating significant computational efficiency advantages.**

Index Terms—**Lithium-ion Batteries; State of Charge (SOC); Wavelet Denoising; Bayesian Optimization; SE-CNN-BiLSTM model**

Manuscript received March 27, 2025; revised May 23, 2025. This work was supported by the Basic Scientific Research Project of Institution of Higher Learning of Liaoning Province (Grant No. LJ222410146054), and Postgraduate Education Reform Project of Liaoning Province (Grant No. LNYJG2022137).

Song-Bo Zhang is a postgraduate student of School of Electronic and Information Engineering, University of Science and Technology Liaoning, Anshan, 114051, P. R. China (e-mail: zsb@stu.ustl.edu.cn).

Jie-Sheng Wang is a professor of School of Electronic and Information Engineering, University of Science and Technology Liaoning, Anshan, 114051, P. R. China (Corresponding author, phone: 86-0412-2538246; fax: 86-0412-2538244; e-mail: wjs@ustl.edu.cn).

Chun-Ni Shi is a teacher of School of Electronic and Information Engineering, University of Science and Technology Liaoning, Anshan, 114051, P. R. China (e-mail: 322028@ustl.edu.cn).

Xiao-Tian Wang is a postgraduate student of School of Electronic and Information Engineering, University of Science and Technology Liaoning, Anshan, 114051, P. R. China (e-mail: wxt@stu.ustl.edu.cn).

Jun-Yu Lu is a postgraduate student of School of Electronic and Information Engineering, University of Science and Technology Liaoning, Anshan, 114051, P. R. China (e-mail:24220812030590@stu.ustl.edu.cn).

I. Introduction

Lithium-ion batteries are integral to contemporary energy systems and find extensive application in sectors such as electric vehicles, portable electronic devices and energy storage solutions [1]. Their high energy density, prolonged cycle life and minimal self-discharge rate render them among the most favored battery technologies available today [2]. In battery management systems, State of Charge (SOC) serves as a critical parameter for assessing the remaining charge of a battery, which directly influences its performance, safety and longevity. Nevertheless, accurately predicting SOC poses significant challenges due to the myriad complex factors that affect batteries during operation, such as temperature fluctuations, varying charging and discharging rates and aging processes [3]. Presently, the predominant methodologies for SOC prediction encompass electrochemical modeling, empirical modeling and data-driven approaches [4]. Electrochemical modeling is grounded in the physical and chemical characteristics of batteries. While it offers high predictive accuracy, it entails considerable computational complexity. Conversely, empirical modeling leverages historical data alongside established formulas. Although straightforward to implement, it tends to exhibit lower accuracy. Data-driven modeling employs machine learning and deep learning techniques that yield commendable predictive performance, but it is susceptible to variations in data quality and model selection.

Existing state-of-charge (SOC) prediction models exhibit numerous limitations in complex dynamic environments. Traditional electrochemical and empirical models struggle to deliver high-precision predictions when confronted with the dynamic characteristics and environmental fluctuations of batteries, primarily because these models typically operate under the assumption of ideal or static conditions, failing to adequately account for the complexities inherent in real-world applications. Although data-driven approaches have enhanced predictive accuracy to some degree, their efficacy is contingent upon the quality of training data and model architecture selection [5]. Furthermore, data noise significantly impacts SOC prediction accuracy. In practical scenarios, battery data often suffers from measurement errors and environmental disturbances that compromise input integrity and undermine prediction reliability. Consequently, effectively mitigating data noise emerges as a critical step toward enhancing SOC prediction precision. Simultaneously,

hyperparameter optimization is vital for improving model performance [6], given that deep learning architectures are particularly sensitive to hyperparameters such as neuron count, learning rate and regularization coefficients [7-8]. The conventional manual tuning of hyperparameters proves both time-consuming and unreliable [9].

Peng et al. proposed an enhanced method for estimating the state of charge (SOC) of lithium-ion batteries, utilizing a cubic Kalman filter (CKF). A first-order RC model and a fractional-order model were developed, with parameters identified through a mixed pulse power characteristic experiment. The CKF demonstrated superior robustness in SOC estimation compared to the extended Kalman filter (EKF). Additionally, the Kalman gain coefficient was refined by using a fuzzy controller, effectively reducing the SOC estimation error to 2% [10]. Chen et al. introduced an advanced battery SOC estimation approach that integrates a feed-forward neural network (FFNN) with the extended Kalman filter. Its robustness across varying temperatures was validated through experimental studies. Hardware-in-the-loop testing indicated that this method could converge to reference values despite initial errors in SOC and capacity, making it suitable for complex electric vehicle environments [11]. Li et al. presented a novel SOC estimation technique based on GRU-RNN architecture, wherein SOC is directly inferred from voltage, current and temperature data without necessitating an internal battery parameter model. This methodology allows for accurate SOC estimations by using a single set of network parameters across different temperature conditions. Results from multiple datasets revealed its accuracy and robustness [12]. Yang et al. proposed a method by utilizing the long short-term memory (LSTM) recurrent neural network to estimate the state of charge (SOC) of lithium iron phosphate batteries across varying temperatures. By integrating this approach with the unscented Kalman filter (UKF) for noise reduction, experimental results indicate that the method achieves an SOC estimation error of less than 1.1% under different thermal conditions, demonstrating its capability to provide accurate estimates even in untrained temperature scenarios [13]. Tian et al. introduced a SOC estimation technique that combines the LSTM network with the adaptive cubic Kalman filter (ACKF). The LSTM effectively captures the nonlinear relationships among SOC, current, voltage and temperature, while the ACKF enhances output smoothing to ensure precise and stable SOC estimations. Notably, this methodology does not necessitate a battery model. Experimental findings reveal significant improvements in estimation accuracy across diverse datasets [14]. Bian et al. developed a bidirectional LSTM encoder-decoder model aimed at estimating the SOC of lithium-ion batteries under various temperatures. This model enhances estimation precision by leveraging contextual information and bidirectional dependencies within measurement sequences, thereby bolstering both reliability and availability of battery management systems in heterogeneous environments [15]. Ren et al. introduced a long short-term memory (LSTM) network optimized through particle swarm optimization (PSO) for the estimation of state of charge (SOC) in lithium-ion batteries. The LSTM parameters were fine-tuned by using PSO, and random noise was incorporated into the input layer to enhance its resilience against interference [16]. Liu et al. developed a SOC estimation method by utilizing a temporal convolutional network (TCN), which operates independently of battery models or adaptive filters, directly mapping accurate SOC from voltage, current and temperature data. This approach is also adaptable to various battery types via transfer learning [17]. Chen et al. proposed an innovative SOC estimation technique that integrates a denoising autoencoder (DAE-NN) with a gated recurrent unit (GRU) recurrent neural network (RNN). The DAE-NN serves to extract features from battery data while mitigating noise. Subsequently, these extracted features are employed to train the GRU-RNN. In comparison to traditional GRU-RNNs, the DAE-GRU demonstrates superior accuracy and robustness in SOC estimation [18]. Yang et al. introduced a deep learning approach leveraging a dual-stage attention mechanism to enhance the accuracy of state-of-charge (SOC) estimation for lithium-ion batteries while mitigating the effects of noise. This method incorporates current, voltage and temperature features into an encoder-decoder network based on gate-controlled recurrent units, employing the attention mechanism to adaptively extract pertinent features and account for temporal sequence correlations [19].

Sun et al. proposed a state-of-health (SOH) prediction method for lead-acid batteries by utilizing a CNN-BiLSTM-Attention model. The convolutional neural network (CNN) was employed to extract features and reduce dimensionality, while the bidirectional long short-term memory (BiLSTM) network captured temporal dependencies in both directions. An attention mechanism was incorporated to emphasize critical features, thereby achieving precise multi-step SOH predictions [20]. Cui et al. introduced a hybrid approach based on a CNN-bidirectional weighted gate recurrent unit (BWGRU), which utilized a 'multi-time-step input' structure alongside BWGRU to optimize the impact of battery information on predictive outcomes. The CNN facilitated the learning of input feature parameters, whereas the BWGRU enhanced fitting performance at low temperatures by dynamically adjusting weights. This network exhibited high accuracy and stability across varying conditions and effectively mitigated the influence of different initial states of charge (SOC) on estimation results [21]. Yan et al. developed an innovative knowledge-constrained convolutional neural network-bidirectional long short-term memory (KCCL) model that demonstrated superior robustness under conditions of limited training data availability. By integrating statistical and physical knowledge constraints into its training framework, this model not only prioritized data point accuracy but also accounted for underlying physical relationships among them, thus enhancing both SOC estimation accuracy and reliability. Evaluation results indicated that the KCCL model outperformed its counterpart lacking knowledge constraints when faced with restricted training datasets [22]. Wang et al. proposed a cloud-edge collaborative approach in which a deep learning model based on CNN-LSTM was implemented in the cloud, while the coulomb counting method and Kalman filter were

employed at the edge. By integrating the estimated results from both ends through the Kalman filtering algorithm, high-precision and real-time state of charge (SOC) online estimation was achieved. Evaluation results indicate that under three dynamic driving scenarios, this method can deliver accurate real-time estimations across varying temperature conditions and initial error states within the network architecture [23].

Xu et al. proposed a CNN-LSTM model that integrates feature selection and skip connections to predict the state of health (SOH) of lithium-ion batteries. The feature selection technique effectively eliminates irrelevant features, thereby enhancing training efficiency and prediction accuracy. Additionally, the incorporation of skip connections addresses the degradation issue associated with multi-layer LSTMs [24]. Rincon-Maya et al. introduced an innovative approach for predicting the remaining useful life (RUL) of lithium-ion batteries by employing individual control charts (ICC) to filter out degraded data, convolutional neural networks (CNN) to mitigate data noise, and long short-term memory networks (LSTM) to capture both spatial and temporal dependencies within the data [25]. Li et al. developed a hybrid methodology that combines deep learning techniques with Kalman filtering for estimating the state of charge (SOC). By integrating convolutional neural networks (CNNs) or temporal convolutional networks (TCNs) with various recurrent neural network variants, including long short-term memory (LSTM), gated recurrent units (GRU), peephole long short-term memory (Peephole LSTM) and bidirectional long short-term memory (BiLSTM), the model captures both spatial and temporal characteristics of input signals. Subsequently, this deep learning framework is augmented with a Kalman filter to mitigate transient signal oscillations, thus improving SOC estimation accuracy. Results indicate that selecting appropriate deep learning methods can significantly enhance SOC estimation precision. Furthermore, combining these methods with Kalman filtering yields even greater accuracy while minimally affecting estimation time [26]. Yu et al. proposed a method for integrating mechanistic knowledge from the battery domain into a deep learning (DL) framework. Initially, simplified electrochemical models were employed to derive physically relevant variables associated with the underlying mechanisms, thereby enhancing the input features of the DL model. Subsequently, a Bayesian optimization-based long short-term memory (LSTM) network was utilized to identify highly correlated variables, which were incorporated into the input to enhance the accuracy of state-of-charge (SOC) estimation. The results demonstrated that this approach could significantly improve SOC estimation performance while incurring only a marginal increase in computational cost; its generalizability was further validated across other DL models [27]. Sherkatghanad et al. introduced a deep learning model that integrates convolutional neural networks (CNN), bidirectional long short-term memory networks (Bi-LSTM) and an attention mechanism (CNN-Bi-LSTM-AM) for precise SOC estimation of lithium-ion batteries over an extensive temperature range. This model effectively captured critical spatial and temporal dependencies, with the attention mechanism contributing to enhanced performance and robustness in low-temperature conditions [28]. Lin et al. developed a capacity prediction method for lithium-ion batteries based on convolutional neural networks (CNN) and bidirectional long short-term memory networks (BiLSTM), optimizing hyperparameters through the swallow optimization algorithm (SSA). This methodology automatically extracted features via CNN while leveraging BiLSTM for capacity forecasting, demonstrating efficacy on public datasets under two distinct temperature scenarios [29].

This paper introduces a robust framework for State of Charge (SOC) prediction by integrating Squeeze-and-Excitation Convolutional Neural Networks (SE-CNN) with Bidirectional Long Short-Term Memory networks (BiLSTM). The proposed method enhances predictive performance through the application of wavelet denoising and Bayesian optimization techniques. The key contributions of this study are as follows:

(1) Propose an SE-CNN-BiLSTM model for lithium-ion battery SOC prediction, leveraging Bayesian optimization and wavelet denoising to enhance both accuracy and robustness.

(2) Wavelet transformation is employed to perform effective denoising on battery data, significantly mitigating measurement errors and environmental noise.

(3) The Squeeze-and-Excitation module within the convolutional neural network (SE-CNN) facilitates feature extraction by dynamically adjusting feature weights, thereby improving the representation efficacy.

(4) Hyperparameters of the BiLSTM model, including neuron count, learning rate and L2 regularization coefficient, are optimized via Bayesian methods to ensure high predictive accuracy and generalization capability in complex dynamic environments.

The structure of the remainder of this paper is organized as follows. The second section introduces a SE-CNN-BiLSTM model for predicting the state of charge (SOC) of lithium-ion batteries, employing Bayesian optimization and wavelet denoising techniques. This includes data noise reduction through wavelet transformation, the design of a convolutional neural network (CNN) integrated with a Squeeze-and-Excitation (SE) module, and the application of Bayesian optimization to enhance a bidirectional long short-term memory network (BiLSTM). The third section presents simulation validation under three distinct temperature conditions: -10°C, 0°C and 10°C, utilizing data from Turnigy Graphene 5000mAh 65C lithium-ion batteries. Finally, the fourth section summarizes the findings and provides concluding remarks.

II. SE-CNN-BiLSTM Lithium-ion Battery SOC Prediction Model Based on Bayesian Optimization and Wavelet Denoising

The proposed Bayes-DWT-CNN-BiLSTM-Attention architecture initially employs the discrete wavelet transform (DWT) to mitigate noise in the original dataset, effectively eliminating interference while preserving essential signal features. Subsequently, a convolutional neural network (CNN) integrated with a squeeze-and-excitation (SE) module is utilized to extract features

from the denoised data, thereby enhancing the model's capacity to assign weights to various features and improving feature representation efficacy. Building upon this foundation, Bayesian optimization is applied to fine-tune parameters such as neuron count, learning rate and L2 regularization coefficient within the BiLSTM framework, ensuring both predictive accuracy and generalizability of the model in complex dynamic environments. Ultimately, these extracted features are fed into the optimized BiLSTM for state-of-charge (SOC) prediction. The overall architecture of this SOC prediction model is illustrated in Fig. 1.

A. Battery Data Set Turnigy Graphene 5000mAh 65C Li-ion

The Turnigy Graphene 5000mAh 65C Li-ion Battery Dataset comprises a series of tests conducted by Dr. Phillip Kollmeyer at McMaster University in Hamilton, Ontario, Canada, focusing on the performance characteristics of a novel 5Ah Turnigy Graphene 5000mAh 65C battery [32]. These evaluations were performed by utilizing a Digatron universal battery tester with an output capacity of 75A and 5V within an eight-cubic-foot thermal chamber, ensuring voltage and current accuracy to within 0.1% of full scale.

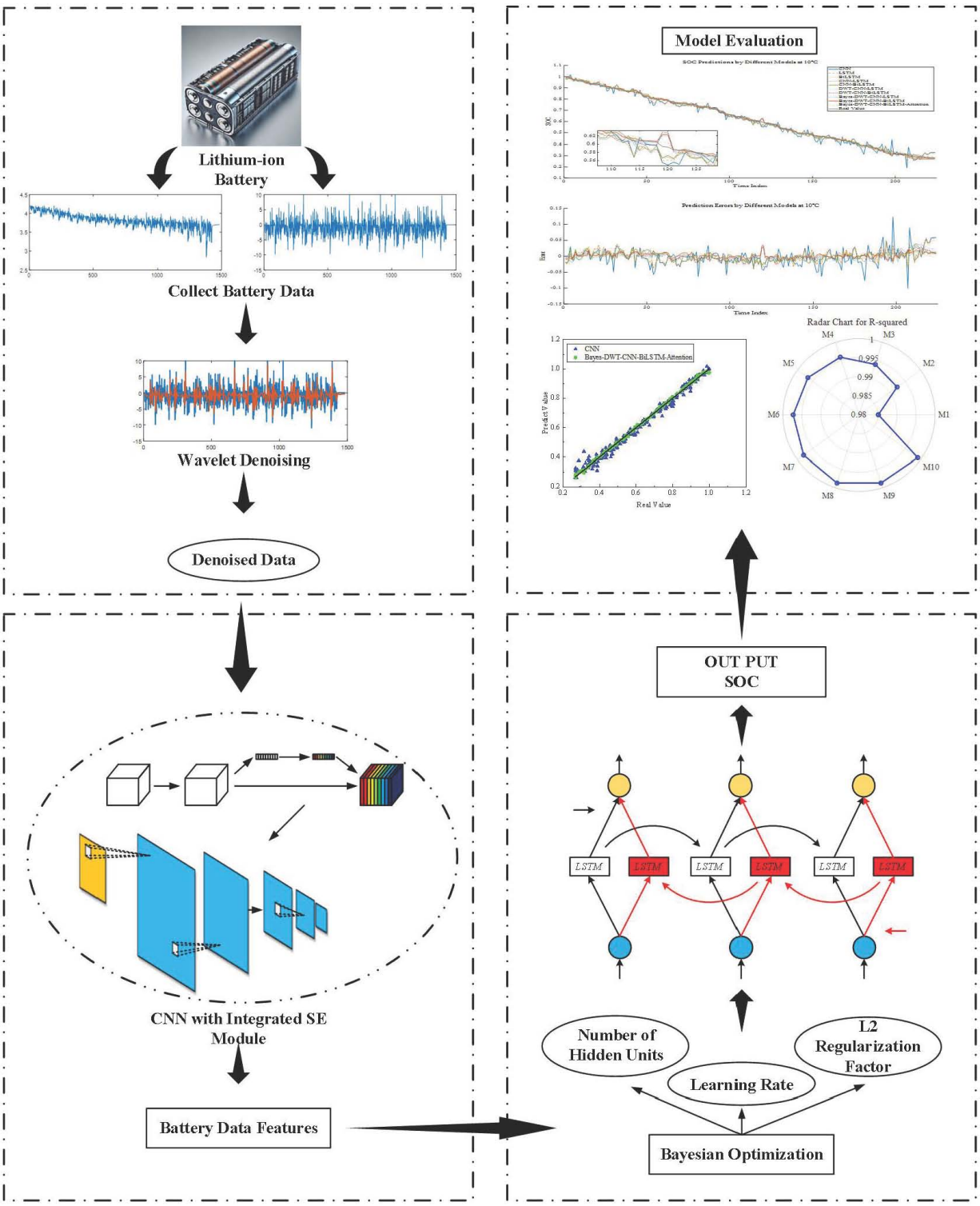

Fig. 1 Overall architecture of the SOC prediction model proposed in this paper.

The experiments were carried out across six distinct ambient temperatures (40°C, 25°C, 10°C, 0°C, -10°C and -20°C) to comprehensively assess the battery's performance metrics. Following each test cycle, the battery was charged at a rate of 1C to reach a voltage of 4.2V with a charge termination current set at 5mA under standard conditions (25°C). The testing regimen included high-power pulse-charge (HPPC) assessments through four-pulse sequences as well as C/20 discharge and charge cycles alongside discharge tests at rates of 0.5C, 2C and 1C. Additionally, UDDS, HWFET, LA92 and US06 driving cycle simulations were executed to evaluate the battery's operational efficacy in compact electric vehicle applications. The data presented herein is derived from the LA92 driving cycle test conducted under ambient temperatures of -10°C, 0°C and 10°C.

B. Wavelet Transform Denoising

When predicting the state of charge (SOC) of lithium-ion batteries, the collected battery data, such as voltage, current and temperature, can be influenced by intricate noise factors, resulting in distorted sensor readings [30]. Given that neural networks exhibit a significant reliance on high-quality data to facilitate effective training and accurate predictions, the presence of noise may lead the network to assimilate irrelevant information, thereby diminishing prediction accuracy. Furthermore, noise can adversely impact the predictability of time-series data. Consequently, implementing robust denoising techniques to enhance data quality is essential for improving the precision of SOC predictions for lithium-ion batteries.

The fundamental principle behind wavelet denoising involves decomposing the signal into various frequency components through wavelet decomposition. Initially, an appropriate wavelet basis function and decomposition level are selected. Subsequently, the signal is decomposed into multiple scales comprising approximate coefficients and detail coefficients [31]. These coefficients undergo thresholding. A predetermined threshold value is established whereby detail coefficients falling below this threshold are set to zero while those exceeding it are preserved. Ultimately, these processed coefficients are reconstructed into a denoised signal via wavelet inverse transform. This methodology effectively mitigates noise from the signal while preserving its principal features.

C. Discrete Wavelet Transform (DWT)

The initial phase of wavelet denoising involves applying the discrete wavelet transform (DWT) to the original data. This process decomposes the original signal into sub-signals across various frequency bands, yielding multiple scales of approximate coefficients and detail coefficients. The selection of suitable wavelet basis functions and decomposition levels is crucial for achieving an effective decomposition [33-34]. Wavelet decomposition effectively concentrates significant features of the signal within a limited number of approximate coefficients while preserving high-frequency noise in the detail coefficients. This frequency-based decomposition facilitates the identification and processing of noise in subsequent stages, thereby establishing a foundation for effective noise removal. In the context of discrete wavelet transform, the signal $x[n]$ is represented as a series of scale coefficients (approximate coefficients) and wavelet coefficients (detail coefficients), as illustrated by the following formula:

$$A_j[k] = \sum_n x[n] \cdot \phi_{j,k}[n] \tag{1}$$

$$\phi_{j,k}[n] = 2^{\frac{-j}{2}} \phi\left(2^{-j} n - k\right) \tag{2}$$

$$D_j[k] = \sum_n x[n] \cdot \psi_{j,k}[n] \tag{3}$$

$$\psi_{j,k}[n] = 2^{\frac{-j}{2}} \psi\left(2^{-j} n - k\right) \tag{4}$$

where, j signifies the decomposition level or scale of the wavelet transform, while k indicates the position of the signal within the time domain. The symbols $A_j[k]$ and $D_j[k]$ correspond to the coefficients of the scale function (approximation coefficients) and wavelet function (detail coefficients), respectively, for the decomposed signal $x[n]$. Additionally, $\phi_{j,k}[n]$ and $\psi_{j,k}[n]$ denote the discrete representations of both the scale function and wavelet function.

D. Noise Reduction Data Analysis and Presentation

Utilize the 'db1' wavelet to decompose the voltage and current signals into five levels. During the denoising procedure, the standard deviation of noise (σ) is estimated by computing the median absolute deviation (MAD) of the detail coefficients. Subsequently, the threshold (thr) is determined by using σ in conjunction with signal length to effectively suppress noise. In processing the detail coefficients, employ the 'wthresh' function for soft thresholding, which mitigates coefficients that fall below this threshold, thereby facilitating efficient denoising. Eq. (5) pertaining to noise standard deviation, threshold determination and soft thresholding are outlined as follows.

$$\sigma = \frac{median\left(\left|D_j - median\left(D_j\right)\right|\right)}{0.6745} \tag{5}$$

where, D_j represents a collection of detail coefficients, and the median absolute deviation (MAD) is employed to estimate the standard deviation of noise due to its robustness against outliers. The coefficient 0.6745 is utilized to convert MAD into an approximation of the standard deviation.

$$thr = \sigma\sqrt{2\log(N)} \tag{6}$$

where, N denotes the length of the signal.

$$\hat{D}_j[k] = sign\left(D_j[k]\right) \cdot \max\left(\left|D_j[k]\right| - thr, 0\right) \tag{7}$$

where, $\hat{D}_j[k]$ denotes the processed detail coefficient, $sign\left(D_j[k]\right)$ signifies the sign of the returned coefficient, and $\max\left(\left|D_j[k]\right| - thr, 0\right)$ indicates that coefficients below a specified threshold are compressed to zero, thereby effectively mitigating noise. The wavelet decomposition analysis of voltage and current signals at varying temperatures is illustrated in Fig. 2.

E. CNN with SE Module

A convolutional neural network (CNN) integrated with a Squeeze-and-Excitation (SE) module is employed to extract features from battery data for predicting the state of charge (SOC) of lithium-ion batteries. The network initially captures features from voltage, current and temperature data through multiple convolutional layers. An SE module is incorporated after each convolutional layer to adaptively recalibrate channel weights based on global information, thereby emphasizing critical features. Following a series of nonlinear activations and feature compression processes, the final SOC prediction is generated via a fully connected layer.

F. Convolutional Neural Networks (CNNs)

Convolutional Neural Networks (CNNs) represent a class of deep learning architectures particularly adept at processing data characterized by grid-like structures, such as images and videos [35]. In the context of predicting the state of charge (SOC) in lithium-ion batteries, CNNs facilitate the analysis of time-series data by autonomously extracting critical features from voltage, current and temperature measurements through convolutional layers, thereby obviating the need for manual feature engineering. Convolutional layers effectively capture edge and texture information via filter applications, while pooling layers downsample the data to preserve essential features that enhance computational efficiency and mitigate overfitting risks. Subsequently, fully connected layers translate these extracted features into SOC predictions, thereby augmenting prediction accuracy.

The adopted convolutional neural network (CNN) architecture comprises multiple layers designed to process input data of size 1x4. Initially, an input layer is established to receive battery data. Subsequently, the network systematically extracts and refines features by alternately stacking convolutional layers, pooling layers and fully connected layers. During the feature extraction phase, the network initiates with a 5x5 convolutional layer featuring 100 filter channels, ensuring that the output dimensions remain invariant through appropriate padding and stride configurations. Following this, a batch normalization layer along with a ReLU activation function is incorporated to enhance model nonlinearity and expedite training processes. The network then employs a second 5x5 convolutional layer containing 70 filter channels, also utilizing padding and stride settings for dimensional consistency. A pooling layer follows to diminish data dimensions while extracting salient features. Further refinement occurs through a series of 3x3 convolutional layers with 50 and subsequently 40 filter channels respectively; each accompanied by ReLU activation functions aimed at capturing more nuanced feature information. Ultimately, all extracted features are forwarded through a fully connected layer to yield the final output prediction as illustrated in Fig. 3.

G. SE Module

Incorporating the Squeeze-and-Excitation Module (SE) into convolutional neural networks significantly enhances their capability to represent features for predicting the state of charge (SOC) in lithium-ion batteries. The SE module improves focus on critical features by adaptively re-normalizing the feature maps derived from battery data. Its fundamental principle involves adjusting channel weights based on global information, thereby amplifying responses to pertinent battery characteristics while attenuating irrelevant or disruptive signals [36-37]. This structural enhancement contributes to increased accuracy in SOC prediction models. A schematic representation of the Squeeze-and-Excitation module is illustrated in Fig. 4.

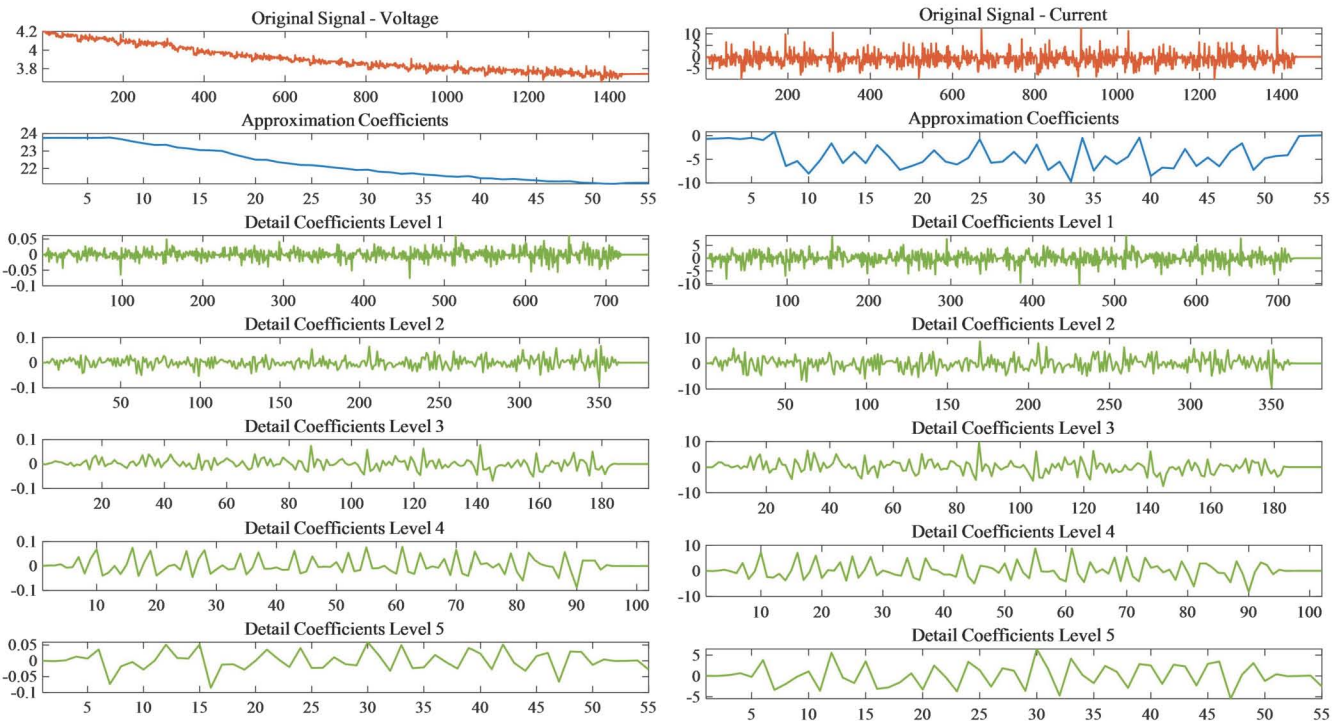

(a) The wavelet decomposition analysis of voltage and current signals at 10°C

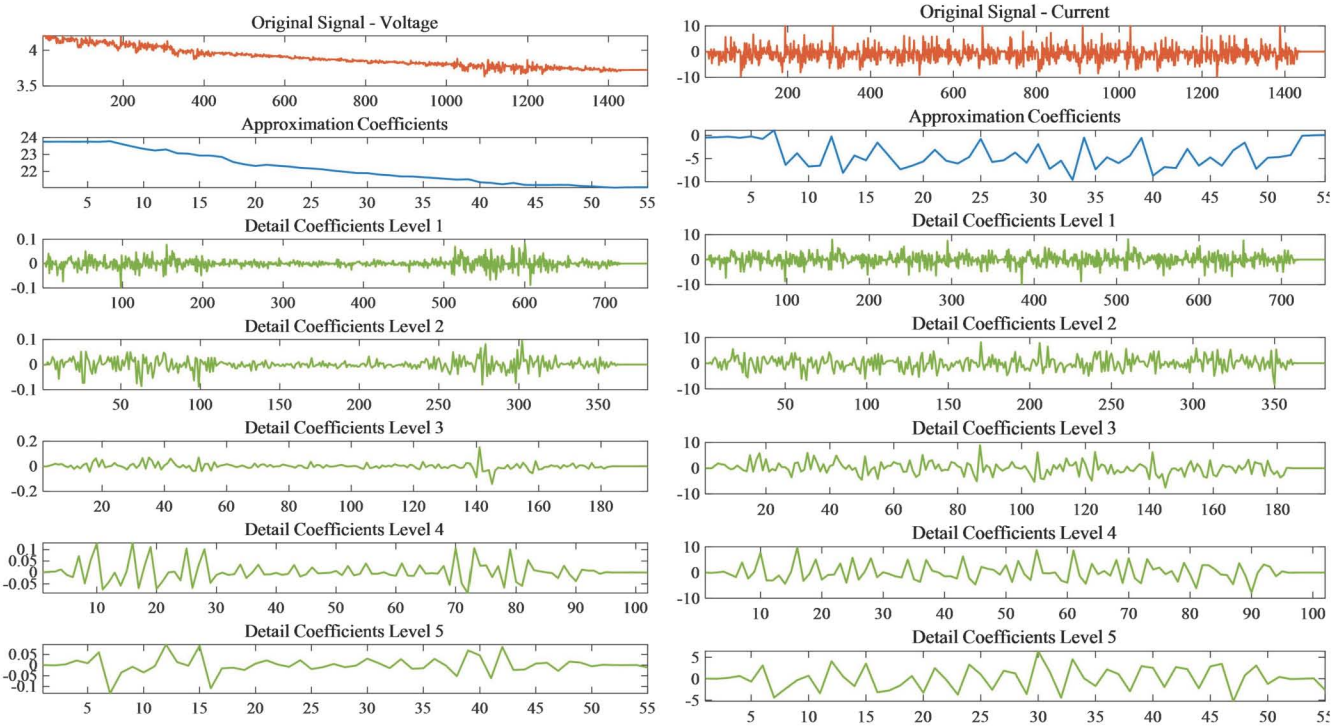

(b) The wavelet decomposition analysis of voltage and current signals at 0°C

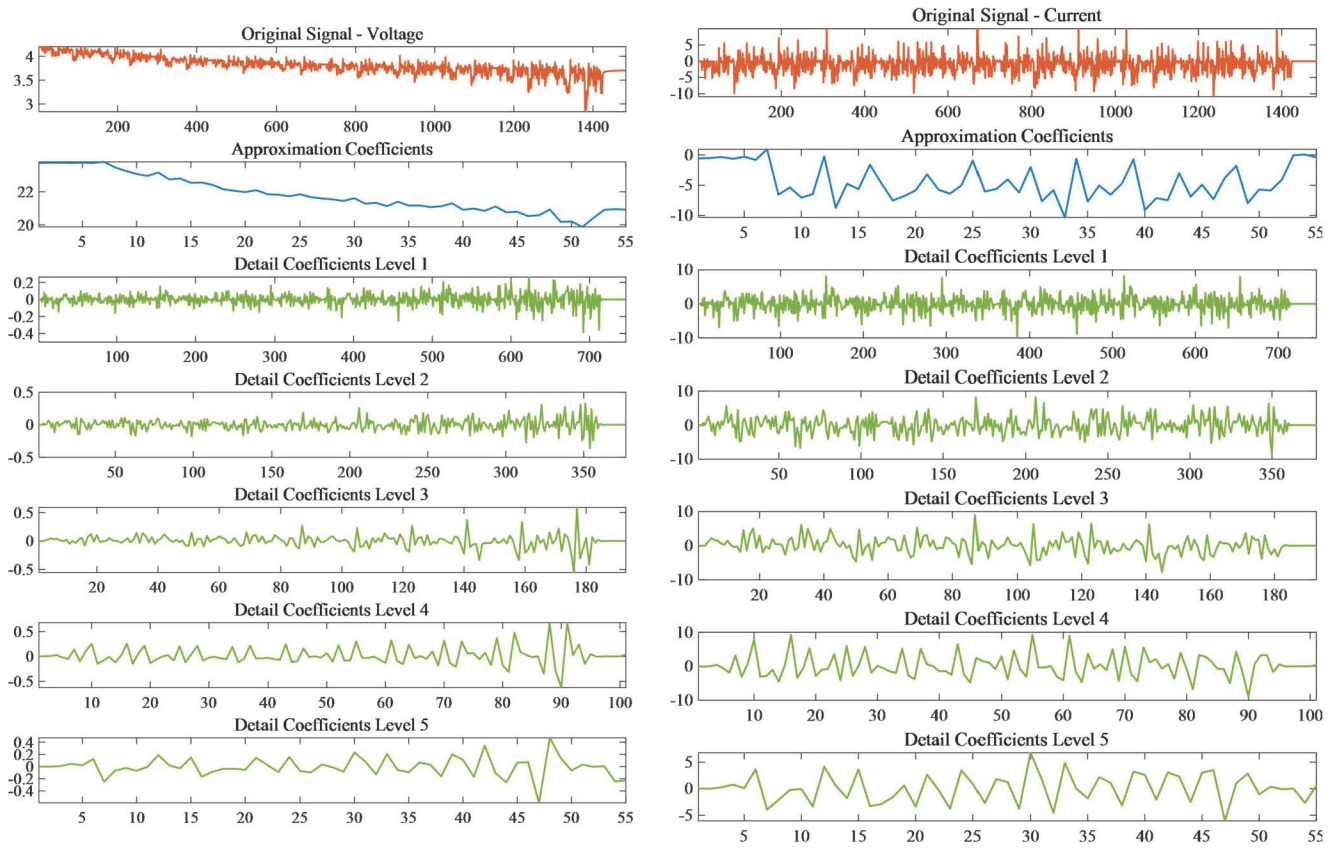

(c) The wavelet decomposition analysis of voltage and current signals at -10°C

Fig. 2 The wavelet decomposition analysis of voltage and current signals at varying temperatures.

The Transformation (F_{tr}) operation serves as a transformation function that converts the input feature map X into the output feature map U . F_{tr} can be interpreted as a conventional convolution operation. The computation process for deriving the output feature map U_c is outlined as follows:

$$U_c = V_c * X = \sum_{s=1}^{C'} V_c^s * X^s \tag{8}$$

Specifically, let X denote the input feature map of dimensions $H' \times W' \times C'$, while U represents the output feature map of dimensions $H \times W \times C$. V_c corresponds to the c th convolution kernel, and V_c^s signifies the parameters associated with the c th convolution kernel on

the s -th input channel. Furthermore, $*$ denotes the convolution operation itself. The right-hand side of this equation illustrates that the output feature map U_c is derived by executing a convolution operation across each channel of the input feature map X and subsequently aggregating these results.

In the Squeeze (Global Information Embedding) stage, the objective of the global average pooling operation (F_{sq}) is to distill each channel's spatial information into a singular scalar value, referred to as the channel descriptor. Specifically, given an input feature map U of size $H \times W \times C$, the global average pooling compresses the spatial information from each channel, which is represented by the $W \times H$ feature map, into a single-channel scalar value, thereby generating an $1 \times 1 \times C$ feature vector of size z . The outcome of this global average pooling process is articulated through Eq. (9). Specifically, z_c represents the component of the feature vector z corresponding to the c th channel, where this value is derived as the average of all spatial feature values across the c th channel.

$$z_c = F_{sq}\left(U_c\right) = \frac{1}{H \times W} \sum_{i=1}^{H} \sum_{j=1}^{W} U_c\left(i, j\right) \tag{9}$$

In the Excitation (adaptive recalibration) operation, the Squeeze-and-Excitation (SE) module captures channel dependencies and enhances feature representation by weighting the significance of each channel. Specifically, the feature vector z , obtained through global average pooling, is fed into two fully connected neural networks. The first layer compresses the dimensionality of z while introducing nonlinearity via a ReLU activation function. Subsequently, the second fully connected layer expands this dimension again and outputs a weight vector s by using a Sigmoid activation function. This weight vector s is then applied element-wise to each channel of the input feature map U , adaptively recalibrating their importance and thereby enhancing the network's capacity to capture critical features. During the Excitation stage, the SE module learns these weight coefficients for feature channels through a fully connected layer combined with an activation function (typically ReLU followed by Sigmoid). These weights serve to adjust either enhance or suppress specific channels' responses within the input feature map.

$$s = F_{ex}\left(z, W\right) = \sigma\left(g\left(z, W\right)\right) = \sigma\left(W_2 \delta\left(W_1 \cdot z\right)\right) \tag{10}$$

where, W_1 and W_2 represent learnable weight matrices, σ denotes the Sigmoid function, s corresponds to the weight coefficients for each channel, and δ signifies the ReLU activation function. Ultimately, the SE module performs an element-wise multiplication of these weight coefficients with the original feature map across channels, resulting in a recalibrated output feature map.

In the Scale (Re-weighting) operation, the objective is to apply the attention weights derived from the preceding Excitation operation to each channel of the feature map. Specifically, for each channel's input feature map U , it is multiplied by its corresponding weight s_c to yield a weighted output feature map $\tilde{X}_c$. This process can be mathematically represented by Eq. (11).

$$\tilde{X}_c = F_{scale}\left(U_c, s_c\right) = s_c \cdot U_c \tag{11}$$

where, U_c represents the feature map corresponding to the c -th channel of the input feature map, while s_c denotes the weight coefficient associated with that channel. Ultimately, the weighted feature map $\tilde{X}_c$ functions as the output of the Squeeze-and-Excitation (SE) module. This operation enables the network to adaptively modulate features according to each channel's significance, thereby enhancing its ability to capture critical information.

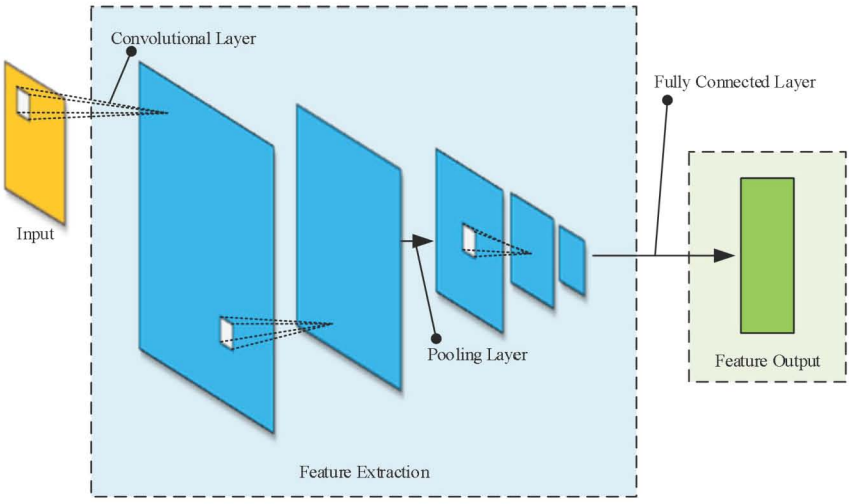

Fig. 3 Architecture diagram of convolutional neural network.

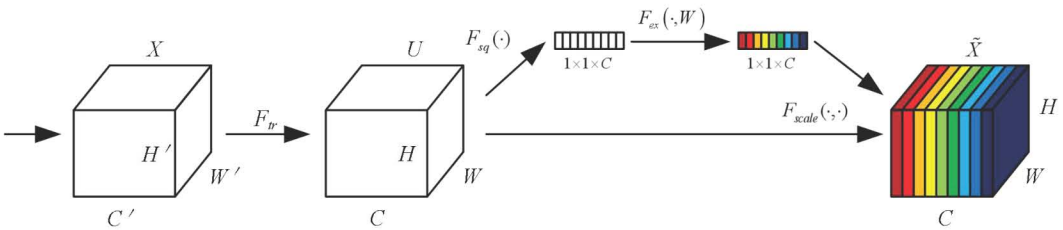

Fig. 4 Structure diagram of the Squeeze-and-Excitation module.

H. Bayesian Optimization with Bidirectional Long Short-Term Memory Neural Network

In the prediction of state-of-charge (SOC) for lithium-ion batteries, the integration of Bayesian optimization with a bidirectional long short-term memory neural network (Bi-LSTM) markedly enhances model performance. The feature outputs derived from a convolutional neural network (CNN) augmented by an SE module will serve as inputs to the Bi-LSTM, further bolstering predictive accuracy. Bayesian optimization adeptly fine-tunes the hyperparameters of the Bi-LSTM architecture, optimizing both its structure and training process to ensure maximal prediction precision. The Bi-LSTM's bidirectional framework effectively captures temporal dependencies in time series data, thereby improving its capacity to model battery voltage, current and temperature dynamics. Through meticulous tuning via Bayesian optimization, the Bi-LSTM model is better equipped to accurately discern dynamic fluctuations in battery SOC, ultimately enhancing both reliability and precision in predictions.

I. Bidirectional Long Short-Term Memory Neural Network (BiLSTM)

The LSTM unit comprises a forget gate (f_t), an input gate (i_t), an output gate (o_t) and a memory cell (C_t). The structural diagram of the LSTM cell is illustrated in Fig. 5. The forget gate is responsible for determining which information within the cell state should be discarded or preserved, while the input gate identifies the new information that needs to be incorporated into the cell state. The output gate regulates the flow of current cell information to the hidden state, ultimately generating the final output [38]. Through these gating mechanisms, Long Short-Term Memory (LSTM) networks effectively manage both the transmission and updating of information. The mathematical formulations for the forget gate, input gate, output gate and cell state update are presented in Eq. (12)-(15).

$$f_t = \sigma\left(w_{fx}x_t + w_{fh}h_{t-1} + b_f\right) \tag{12}$$

$$i_t = \sigma\left(w_{ix}x_t + w_{ih}h_{t-1} + b_i\right) \tag{13}$$

$$o_t = \sigma\left(w_{ox}x_t + w_{oh}h_{t-1} + b_o\right) \tag{14}$$

$$s_t = tanh\left(w_{cx}x_t + w_{ch}h_{t-1} + b_c\right) \tag{15}$$

where, the subscripts w and b denote the weight matrices and bias vectors associated with the forget gate, input gate and output gate, respectively. The function σ is a Sigmoid activation function that produces an output ranging from 0 to 1, serving as a gating mechanism where 0 signifies discarding information and 1 indicates retention. s_t represents the common candidate value vector within layer $tanh$.

The update mechanism for the cell state is delineated as follows. Initially, the forget gate identifies and selects the portions of the previous cell information that are to be discarded, multiplying the old state by the output of the forget gate f_t to eliminate unnecessary data retention. Subsequently, new candidate cell information s_t is introduced via the input gate, which is then scaled by the output of this input gate i_t to derive a new cell state C_t . This process is illustrated through corresponding formulas alongside those governing LSTM unit outputs.

$$C_t = f_t C_{t-1} + i_t s_t \tag{16}$$

$$h_t = o_t tanh(C_t) \tag{17}$$

The computational mechanisms of each neural cell are delineated in Eq. (18)-(19), where σ denotes the activation function, u , v and w signify the connection weights, and b_1 and b_2 represent the bias values.

$$h_t = \sigma\left(u \cdot x_t + w \cdot h_{t-1} + b_1\right) \tag{18}$$

$$y_t = \sigma\left(v \cdot h_t + b_2\right) \tag{19}$$

The Bidirectional Long Short-Term Memory (BiLSTM) network represents an enhancement of the traditional LSTM model, enabling simultaneous consideration of both forward and backward information flows within the input sequence. By integrating outputs from both forward and backward LSTM networks, BiLSTM effectively captures contextual information in sequence data more comprehensively, thereby enhancing performance in various tasks such as sequence classification, speech recognition and natural language processing [39]. Fig. 6 illustrates the information transmission processes occurring in both forward and backward neural networks across three consecutive time steps. The black lines denote the forward flow of information, while the red lines indicate the reverse flow. The training protocols for these two LSTMs are fundamentally similar; one is trained to process data in a forward direction while the other operates in reverse. As depicted in Fig. 6, these two directional LSTMs function independently without interference during operation. The outputs generated by both hidden layers and output layers from each network will be jointly considered for final results. The specific calculation formula is presented as follows.

$$\vec{h}_t = \sigma\left(\vec{u} \cdot x_t + \vec{w} \cdot \vec{h}_{t-1} + \vec{b}\right) \tag{20}$$

$$\overleftarrow{h}_t = \sigma\left(\overleftarrow{u} \cdot x_t + \overleftarrow{w} \cdot \overleftarrow{h}_{t-1} + \overleftarrow{b}\right) \tag{21}$$

$$y_t = \sigma\left(v \cdot \left[\vec{h}_t; \overleftarrow{h}_t\right] + c\right) \tag{22}$$

where, b and c denote the bias parameters, σ signifies the activation function, u and w represent the weight matrices of connections, while the final output y_t is derived from the integration of outputs produced by both LSTMs.

The operational framework of BiLSTM encompasses three distinct phases. Firstly, the forward and backward LSTM networks are independently trained utilizing the backpropagation through time (BPTT) algorithm; Secondly, at each temporal step, the forward and backward LSTMs process sequence information in isolation; Finally, the outputs from both directions are amalgamated to yield the final predictive outcome. This bidirectional processing approach allows BiLSTM to more comprehensively capture contextual information within the input sequence.

J. Bayesian Optimization

In the context of state-of-charge (SOC) prediction for lithium-ion batteries, the hyperparameters of the BiLSTM model, including the number of hidden neurons, initial learning rate and L2 regularization coefficient, significantly influence both the model's generalization capability and its overall performance. An excessively high number of hidden neurons may lead to over-fitting on training data, thereby diminishing predictive accuracy on unseen battery datasets. Conversely, a too-low count may hinder the model's ability to adequately capture essential features within the battery data, resulting in suboptimal predictions. The selection of an appropriate initial learning rate is equally critical; A learning rate that is too high can impede effective convergence while one that is too low may prolong training or trap it in local optima. Furthermore, the L2 regularization coefficient serves a vital function in mitigating over-fitting by incorporating a weight penalty term into the loss function. However, improper calibration of this coefficient could impair the model's learning capacity and adversely affect SOC prediction accuracy.

To enhance the alignment of the BiLSTM network model with specific datasets, accelerate training speed, and effectively boost model performance, identifying the optimal combination of hyperparameters has emerged as a significant and challenging endeavor. Bayesian optimization techniques are extensively employed due to their ability to integrate prior knowledge with historical evaluation results, facilitating efficient exploration of multi-dimensional parameter spaces and swiftly pinpointing optimal hyperparameter configurations.

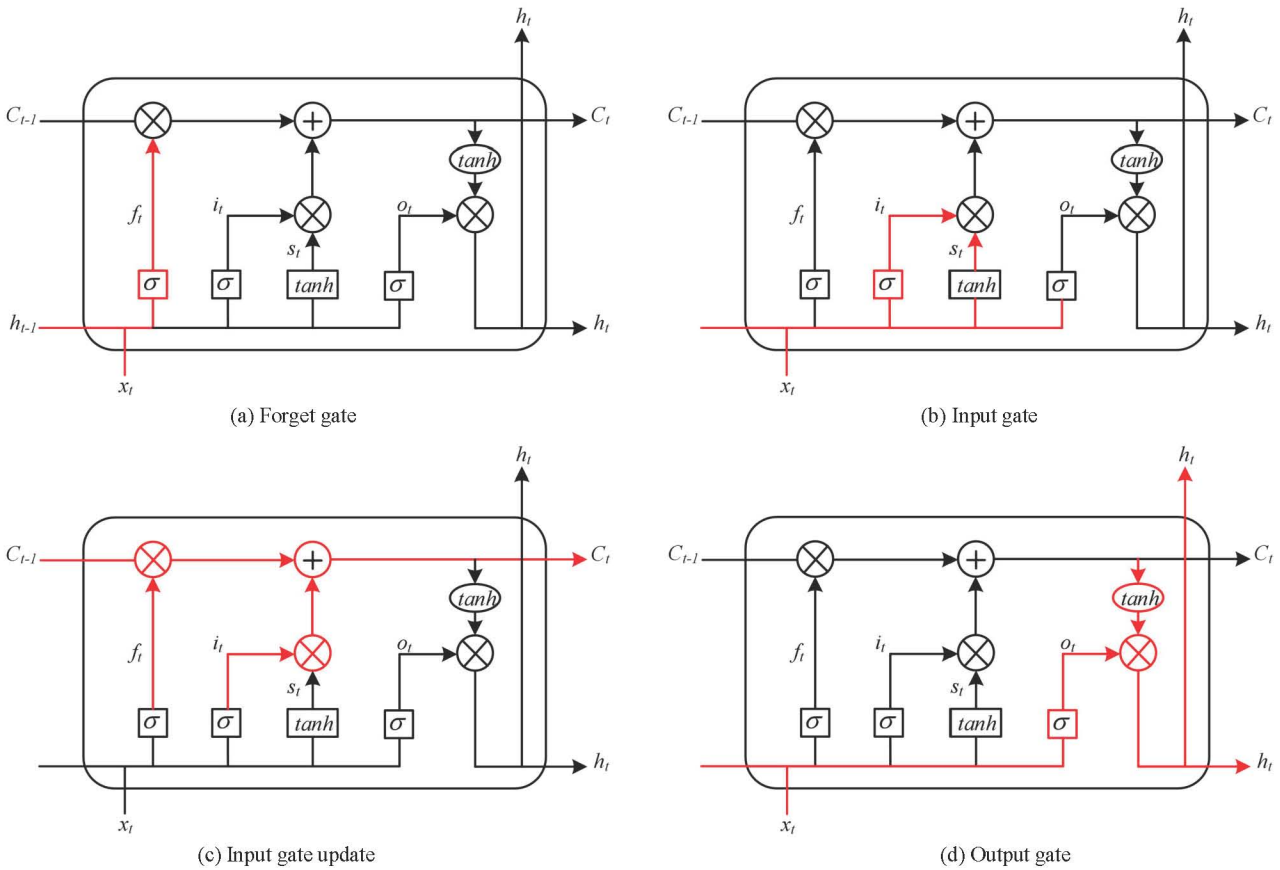

Fig. 5 Schematic diagram of the LSTM cell.

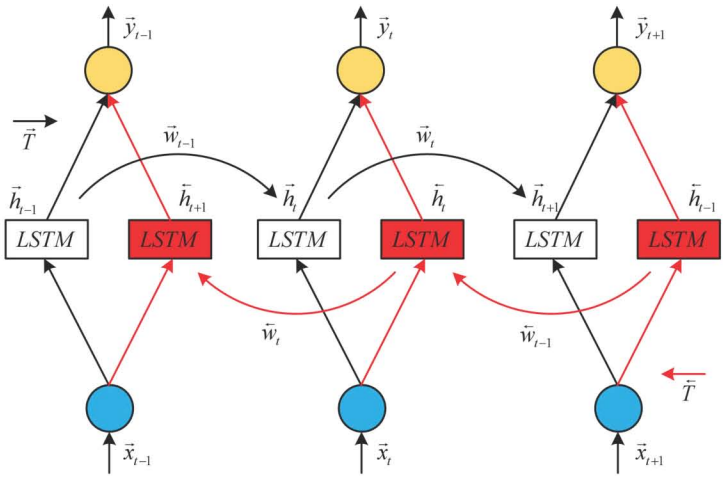

Fig. 6 Architecture of the BiLSTM model.

By leveraging Bayesian optimization, it is possible to reduce the number of iterations while maximizing model performance, thereby ensuring that the network mitigates over-fitting while retaining its capacity to capture intricate data patterns. This approach ultimately enhances the model's generalization capabilities in practical applications.

Bayesian optimization is a highly effective global optimization technique, particularly well-suited for high-dimensional and computationally intensive optimization challenges associated with target functions [40-41]. In the context of optimizing hyperparameters for the BiLSTM model, Bayesian optimization constructs an agent model, typically a Gaussian process, to estimate the distribution of the target function, thereby facilitating an efficient exploration and utilization of the hyperparameter space. This approach leverages information from previously sampled points to iteratively enhance the performance of the target function until optimal hyperparameters are identified. Following each evaluation, the algorithm proceeds to conduct subsequent sampling, enabling it to converge towards an optimal solution while minimizing evaluation costs.

The model delineates a collection of hyperparameter combinations, denoted as $\chi = x_1, x_2, \cdots, x_n$, while Eq. (23) articulates the mathematical framework for identifying the optimal hyperparameter combination within the model.

$$x^* = \arg\min_{x \in \chi} f(x) \tag{23}$$

where, x^* denotes an optimized set of hyperparameters, while $f(x)$ signifies the minimization of the target function associated with hyperparameter x within the framework of Bayesian optimization. During this process, the posterior probability of the target function is computed utilizing Bayes' theorem, as illustrated in Eq. (24).

$$P(f|D) = \frac{P(D|f)P(f)}{P(D)} \tag{24}$$

where, f denotes an unknown objective function and constitutes a set of observed data, $P(f|D)$ signifies the posterior probability of the target function f given the observed data D, $P(f)$ represents the prior probability associated with the objective function f, $P(D|f)$ indicates the probability distribution of the observed data under the assumption that f holds true, and $P(D)$ reflects the marginal likelihood distribution. In Bayesian optimization, marginal likelihood plays a crucial role in optimizing hyperparameters. The structure of the predictive model is illustrated in Fig. 7.

III. Simulation Experiment and Result Analysis

A. Simulation Experiment Overview

This section aims to rigorously evaluate and analyze the performance of the Turnigy Graphene 5000mAh 65C lithium-ion battery across varying temperature conditions. Three temperature environments of -10°C, 0°C and 10°C were selected to test the battery's behavior under different temperature conditions and the accuracy of the prediction model. Through simulation, it can be obtained curves representing state of charge (SOC) predictions from various models, followed by an evaluation of prediction errors at different temperatures for each model. Additionally, a radar chart was constructed as a performance indicator to illustrate the comprehensive capabilities of each model. To further substantiate the predictive capacity of these models, scatter plots were generated to visualize correlations between predicted outcomes and actual data points. The visualization of experimental data will facilitate our understanding of how battery performance trends vary with temperature fluctuations while optimizing the prediction model within the battery management system to enhance reliability and accuracy in diverse environmental contexts.

B. Prediction Accuracy Indicator

In assessing the accuracy of a battery performance prediction model, employing multiple metrics for prediction accuracy can yield a more comprehensive understanding. The following four metrics are commonly utilized: root mean square error (RMSE), mean absolute error (MAE), coefficient of determination (R^2) and mean absolute percentage error (MAPE). Each of these metrics emphasizes different aspects and provides insights into the predictive performance from various perspectives.

Root Mean Square Error (RMSE) quantifies the standard deviation of the discrepancies between predicted and actual values, thereby providing a comprehensive assessment of model prediction accuracy. RMSE is particularly sensitive to outliers, making it an effective metric for evaluating model performance under extreme conditions. The formula for RMSE is as follows:

$$RMSE = \sqrt{\frac{1}{n}\sum_{i=1}^{n}(y_i - \hat{y}_i)^2} \tag{25}$$

where, y_i denotes the actual value, $\hat{y}_i$ signifies the predicted value and n indicates the sample size. Given that the unit of RMSE aligns with that of the data, it offers a clear representation of the absolute magnitude of prediction error. A lower RMSE value reflects greater predictive accuracy.

Mean Absolute Error (MAE) represents the average of the absolute deviations between predicted and actual values. In contrast to Root Mean Square Error (RMSE), MAE exhibits reduced sensitivity to individual large discrepancies, thereby offering a more robust estimation of overall error. The formula for MAE is as follows:

$$MAE = \frac{1}{n}\sum_{i=1}^{n}|y_i - \hat{y}_i| \tag{26}$$

In the computation of Mean Absolute Error (MAE), the absolute value is utilized to prevent cancellation due to error direction, thereby providing a more accurate representation of the deviation between predicted and actual values. A lower MAE indicates a reduced average absolute error in the model's predictions, which correlates with enhanced predictive accuracy.

The coefficient of determination, denoted as R^2, quantifies the degree to which the model accounts for variability in the data and serves as an indicator of the model's goodness of fit. The value of R^2 ranges from 0 to 1, where a value of 1 signifies that the model fully captures all variability in the data, while a value of 0 indicates that it fails to account for any variability.

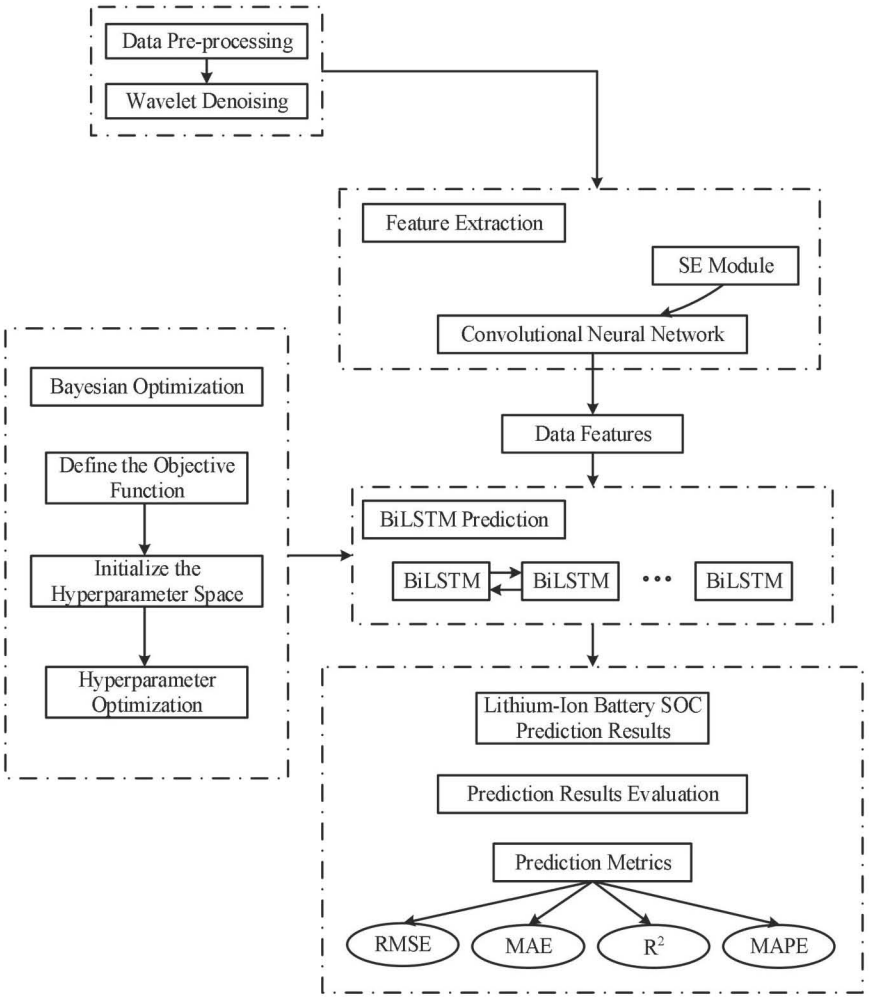

Fig. 7 Structure diagram of SOC prediction model.

The corresponding formula is:

$$R^2 = 1 - \frac{\sum_{i=1}^{n}\left(y_i - \hat{y}_i\right)^2}{\sum_{i=1}^{n}\left(y_i - \overline{y}\right)^2} \tag{27}$$

where, $\overline{y}$ denotes the mean of the observed values, while R^2 provides insight into the model's explanatory power regarding the data. A value closer to 1 indicates a superior fit of the model to the data and an enhanced capacity to account for its variability.

The Mean Absolute Percentage Error (MAPE) is an unscaled metric that quantifies the average percentage of absolute deviations between predicted and actual values. This metric offers a relative assessment of prediction error in relation to actual values, thereby facilitating comparability of errors across diverse data scales. The formula for MAPE is as follows:

$$MAPE = \frac{1}{n}\sum_{i=1}^{n}\left|\frac{y_i - \hat{y}_i}{y_i}\right| \times 100\% \tag{28}$$

MAPE quantifies the proportion of the actual value represented by the prediction error. A lower MAPE indicates a reduced relative prediction error and enhanced predictive accuracy of the model. This metric is particularly valuable for assessing the comparative performance of models across datasets of varying sizes.

By employing a comprehensive set of prediction accuracy metrics, one can thoroughly assess the performance of the predictive model, discern its strengths and weaknesses, and subsequently optimize it. These metrics facilitate enhancements in the model's predictive accuracy within practical applications, thereby bolstering the reliability of battery performance forecasts.

C. Lithium-ion Battery SOC Prediction at 10°C

The simulation experiment results for the state of charge (SOC) of lithium-ion batteries at 10°C, as illustrated in Fig. 8-11, indicate that the SOC prediction curves across all models closely align with actual values. Notably, the prediction curve generated by the Bayes-DWT-CNN-BiLSTM-Attention model demonstrates a significantly closer fit to these actual values, reflecting superior predictive accuracy. This is particularly evident during substantial fluctuations in SOC values, where this model exhibits reduced amplitude in curve variations, underscoring its enhanced adaptability and predictive capability. To further assess comparative prediction accuracy among models, Fig. 9 presents error curves for various approaches. Here, the Bayes-DWT-CNN-BiLSTM-Attention model shows minimal fluctuation in error and a more concentrated overall error distribution. Additionally, Fig. 10 provides a scatter plot comparison between different models and the Bayes-DWT-CNN-BiLSTM-Attention model at 10°C. It is apparent that predictions from this latter model are more tightly clustered around actual values with denser point distributions,

especially when contrasted with traditional CNN and LSTM models, highlighting its stability and precision. Table I quantitatively delineates performance disparities among various models. Notably, the Bayes-DWT-CNN-BiLSTM-Attention model excels across all performance metrics, including RMSE, MAE, MAPE and R^2 values, further substantiating its status as an optimal modeling approach. Furthermore, Fig. 11 illustrates a bar chart depicting each model's performance indicators. Analysis reveals that the Bayes-DWT-CNN-BiLSTM-Attention model achieves superior outcomes across RMSE, MAE, R^2 and MAPE metrics, with particular distinction noted in RMSE and MAPE, thereby affirming its exceptional predictive capacity and robustness.

At 10°C, the Bayes-DWT-CNN-BiLSTM-Attention model demonstrated substantial enhancements across all performance metrics when compared to alternative models. Specifically, the integration of CNN with BiLSTM resulted in reductions of RMSE, MAE and MAPE by 52.24%, 46.43% and 51.58%, respectively, while R^2 was improved by 1.17%. Following the incorporation of DWT denoising techniques, RMSE, MAE and MAPE were further decreased by 22.66%, 28.57% and 22.52% respectively; R^2 saw an enhancement of 0.14%. Subsequent optimization through Bayesian methods led to additional reductions in RMSE, MAE and MAPE by 21.21%, 22.67% and 27.12% respectively; R^2 experienced a modest improvement of 0.07%. Finally, the inclusion of the SE module contributed to further decreases in RMSE, MAE and MAPE by 15.38%, 10.34% and 16.40% respectively; R^2 was enhanced by an additional increment of 0.04%. Collectively, these optimizations markedly elevated both prediction accuracy and stability within the model framework, demonstrating that each optimization step yielded varying degrees of improvement in predictive performance particularly concerning error mitigation and fitting precision.

D. Lithium-ion Battery SOC Prediction at 0°C

The simulation results for the state of charge (SOC) of lithium-ion batteries at 0°C, as illustrated in Fig. 12-15, indicate that the SOC prediction curves across all models closely align with actual values. Notably, the prediction curve generated by the Bayes-DWT-CNN- BiLSTM-Attention model exhibits a remarkable consistency with observed data, demonstrating superior predictive accuracy. This is particularly evident during significant fluctuations in SOC values, where the amplitude of variation in this model's curve is distinctly reduced, highlighting its enhanced performance. To provide a more comprehensive comparison of predictive accuracy among models, Fig. 13 presents error curves for each approach; It reveals that the Bayes-DWT-CNN-BiLSTM-Attention model experiences minimal error fluctuation and displays a more concentrated error distribution. Furthermore, Fig. 14 employs scatter plots to compare model performances at 0°C; Here too, predictions from the Bayes-DWT-CNN- BiLSTM-Attention model show optimal alignment with actual measurements and exhibit denser point distributions. Table II quantitatively assesses differences in predictive performance across models; Findings indicate that the Bayes-DWT-CNN-BiLSTM-Attention model excels in metrics such as RMSE, MAE, MAPE and other error indicators while achieving peak R^2 values, further substantiating its designation as the optimal modeling approach. Lastly, Fig. 15's bar chart corroborates these findings by illustrating that this model surpasses all comparative models across key performance indicators.

At 0°C, the integration of CNN with BiLSTM resulted in reductions of 44.79%, 39.13% and 46.91% in RMSE, MAE and MAPE, respectively, while R^2 exhibited an improvement of 1.19%. The subsequent incorporation of DWT further decreased RMSE, MAE and MAPE by 44.03%, 48.57% and 41.21%, respectively, alongside a modest enhancement in R^2 by 0.35%. Optimization through Bayesian methods led to reductions of RMSE, MAE and MAPE by 20.22%, 22.22% and 25.96% respectively; However, the increase in R^2 was marginal at just 0.06%. Finally, the addition of the SE module contributed to further decreases in RMSE (11.27%), MAE (10.71%) and MAPE (14.52%), with a slight improvement in R^2 by only 0.02%.

E. Lithium-ion Battery SOC Prediction at -10°C

The simulation experimental results for the State of Charge (SOC) of lithium-ion batteries at -10°C, as illustrated in Fig. 16-19, indicate that the prediction accuracy of the Bayes-DWT-CNN-BiLSTM-Attention model is markedly superior, with a reduced fluctuation amplitude in its curve, thereby demonstrating its exceptional performance. To further evaluate the predictive capabilities of various models, Fig. 17 presents the error curves associated with each model. The findings reveal that the Bayes-DWT-CNN-BiLSTM-Attention model exhibits the least error fluctuation and a higher concentration of errors. Additionally, Fig. 18 provides a comparative analysis of each model's performance at -10°C through scatter plots. The prediction outcomes from the Bayes-DWT-CNN-BiLSTM-Attention model align most closely with actual values; furthermore, points within the scatter plot are more densely clustered, reflecting its superior stability.

As illustrated in Table III, the model's performance has undergone significant enhancement at -10°C following multiple optimization strategies. Initially, the integration of CNN with BiLSTM resulted in reductions of RMSE, MAE and MAPE by 51.56%, 40.28% and 48.26% respectively, while R^2 experienced an improvement of 0.70%. Subsequently, the incorporation of wavelet denoising (DWT) further decreased RMSE, MAE and MAPE by 10.09%, 11.63% and 20.89% respectively; R^2 saw a modest increase of 0.04%. Following Bayes optimization, RMSE, MAE and MAPE were reduced by an additional 19.39%, 19.74% and 24.58% respectively with a slight enhancement in R^2 by 0.06%. Finally, the addition of the SE module led to further reductions in RMSE (31.65%), MAE (36.07%) and MAPE (36.35%) along with another increment in R^2 by 0.06%. Fig. 19 provides a clear comparative analysis of each performance metric. As each optimization step is implemented, both prediction accuracy and stability are markedly improved across all indicators, culminating in optimal performance for the Bayes-DWT-CNN-BiLSTM-Attention model at -10°C.

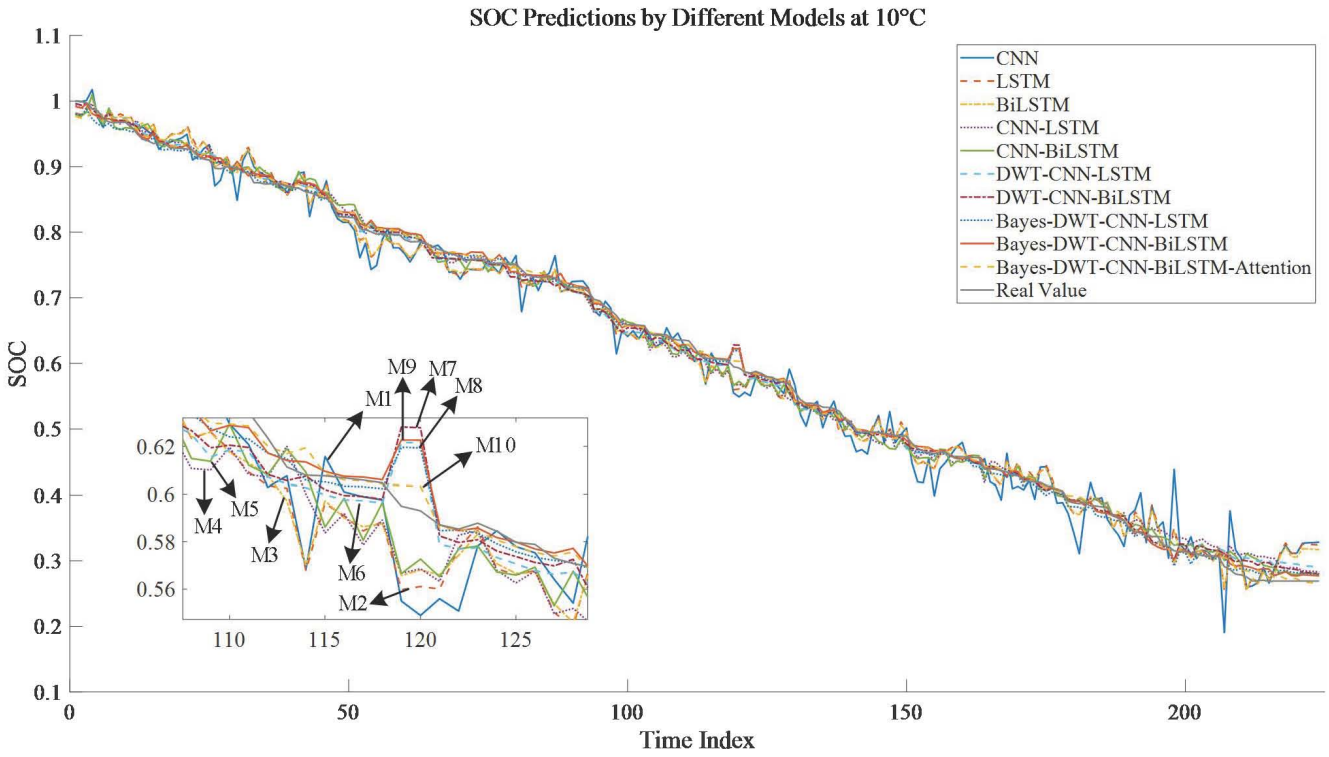

Fig. 8 SOC prediction curves for different models at 10°C.

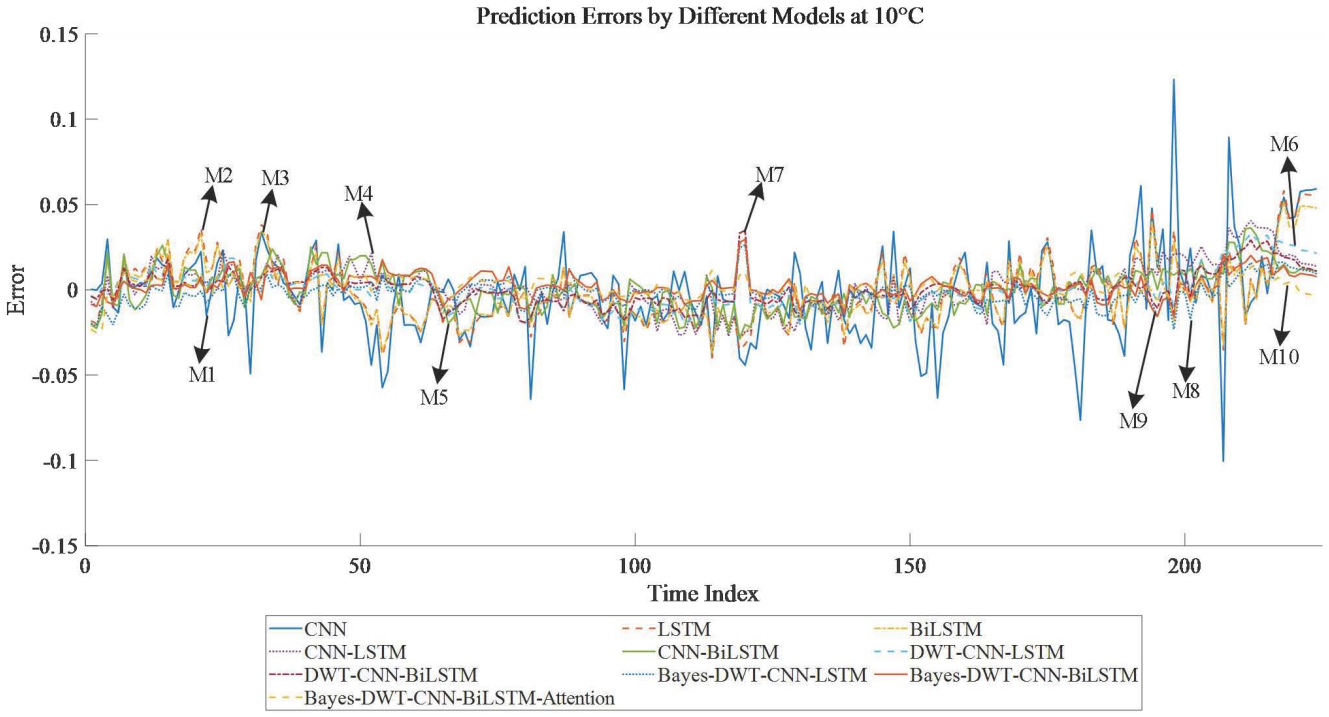

Fig. 9 Predicted error curves for different models at 10°C.

To enhance the persuasiveness of this study, the proposed overall architecture predictive model was rigorously compared with several relevant studies through experimental evaluations, as detailed in Table IV and Fig. 20. This comparison includes the Extended Kalman Filter (EKF), the Adaptive Extended Kalman Filter with Adaptive Fading Factor (MAEKF), the Kalman Filter utilizing an Improved Davidon Equivalent Circuit Model (ECM) and the Genetic Algorithm Support Vector Regression Model (GASVR) under varying cycle conditions and temperatures. The results indicate that the proposed model consistently outperforms these comparative benchmarks, thereby demonstrating that the Bayes-DWT-CNN-BiLSTM-Attention model exhibits superior performance relative to other models.

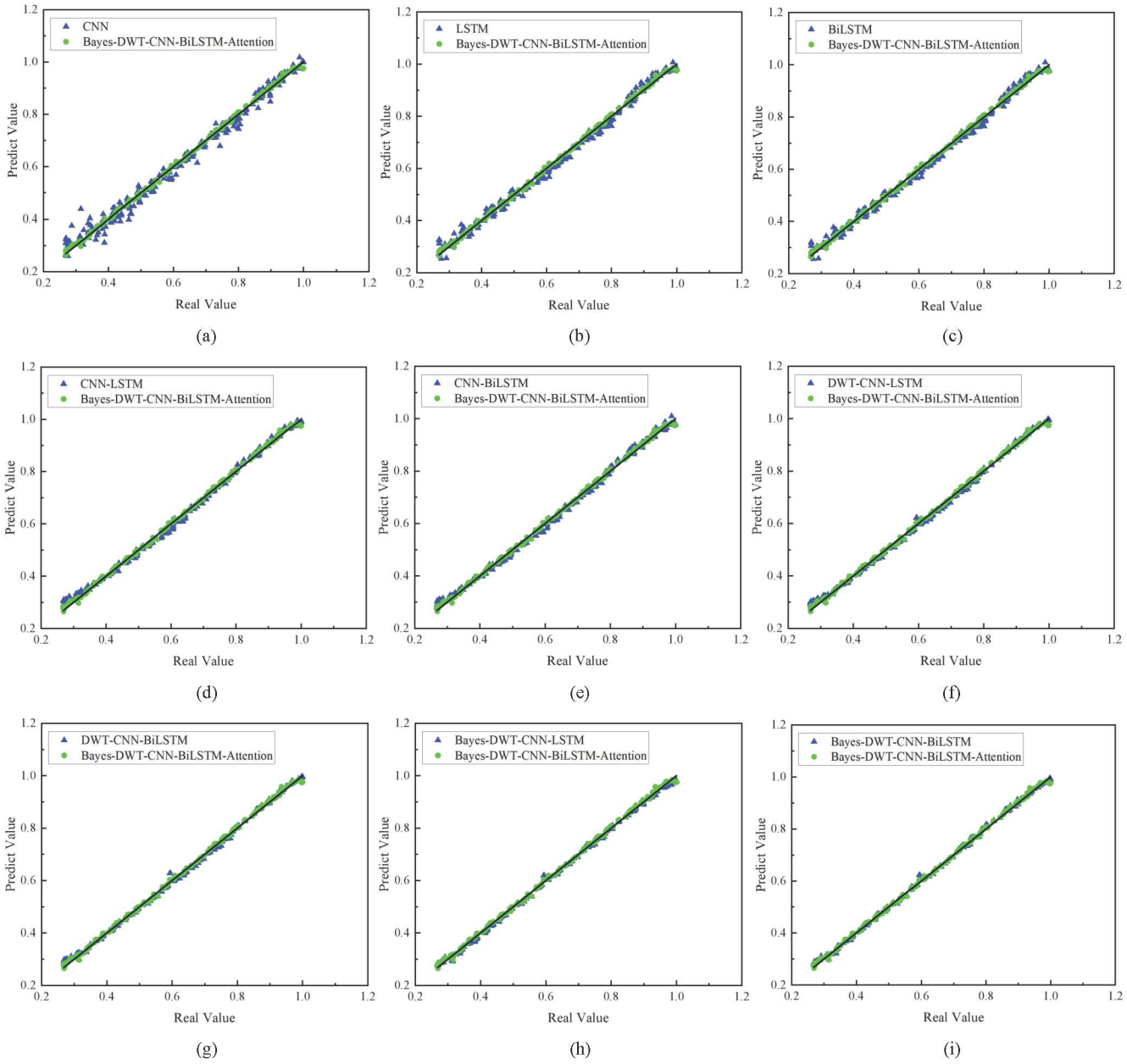

Fig. 10 Scatter plot of different prediction models at 10°C.

TABLE I. PERFORMANCE INDICATORS OF DIFFERENT MODELS AT 10°C

Model	Number	RMSE	MAE	R-squared	MAPE
CNN	M1	0.0268	0.0196	0.9851	4.2357
LSTM	M2	0.0191	0.0151	0.9924	3.0243
BiLSTM	M3	0.0171	0.0137	0.9939	2.7234
CNN-LSTM	M4	0.0140	0.0112	0.9959	2.3972
CNN-BiLSTM	M5	0.0128	0.0105	0.9966	2.0509
DWT-CNN-LSTM	M6	0.0114	0.0086	0.9973	1.8793
DWT-CNN-BiLSTM	M7	0.0099	0.0075	0.9980	1.5891
Bayes-DWT-CNN-LSTM	M8	0.0080	0.0059	0.9987	1.2262
Bayes-DWT-CNN-BiLSTM	M9	0.0078	0.0058	0.9987	1.1581
Bayes-DWT-CNN-BiLSTM-Attention	M10	0.0066	0.0052	0.9991	0.9682

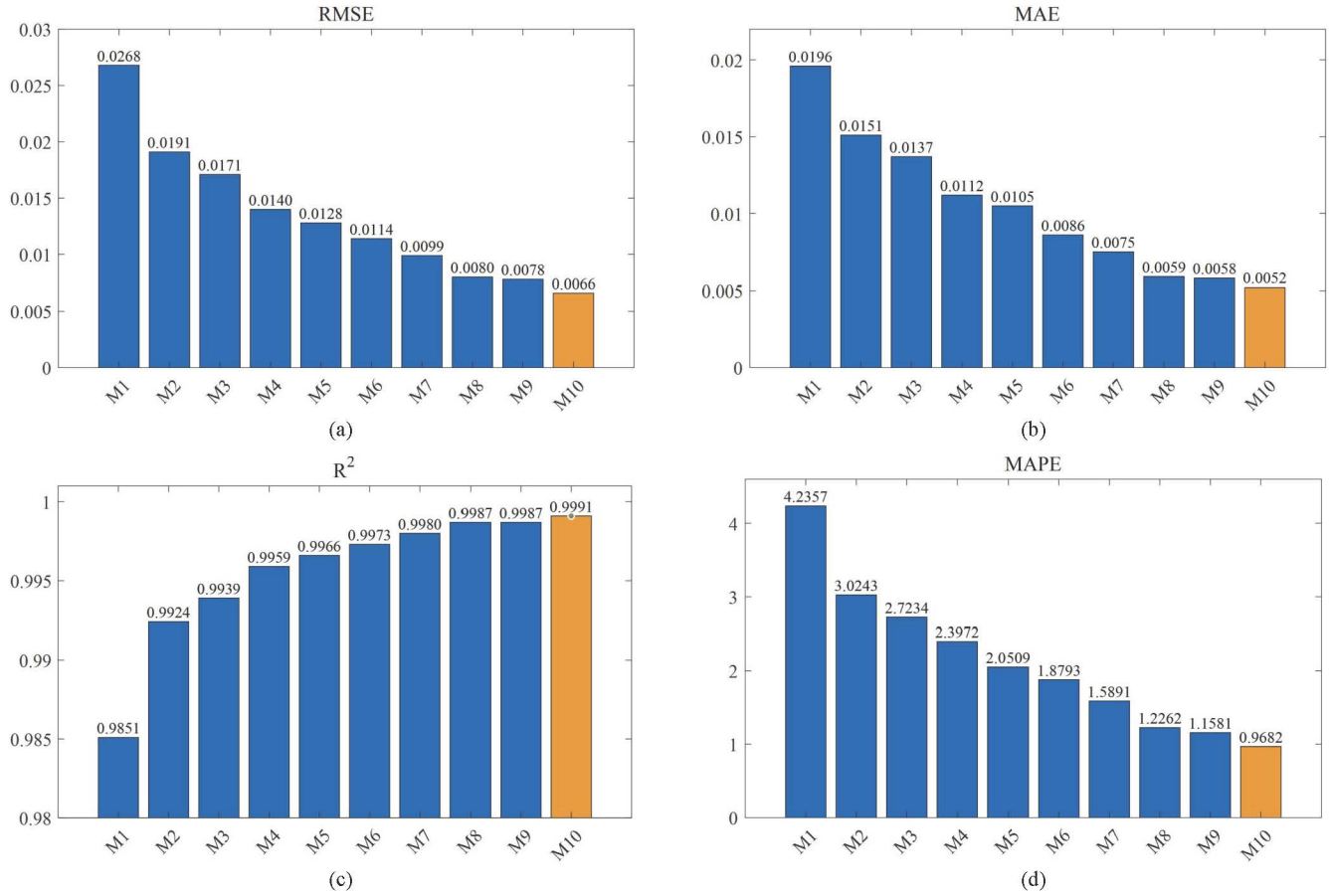

Fig. 11 Bar chart of performance indicators of different prediction models at 10°C.

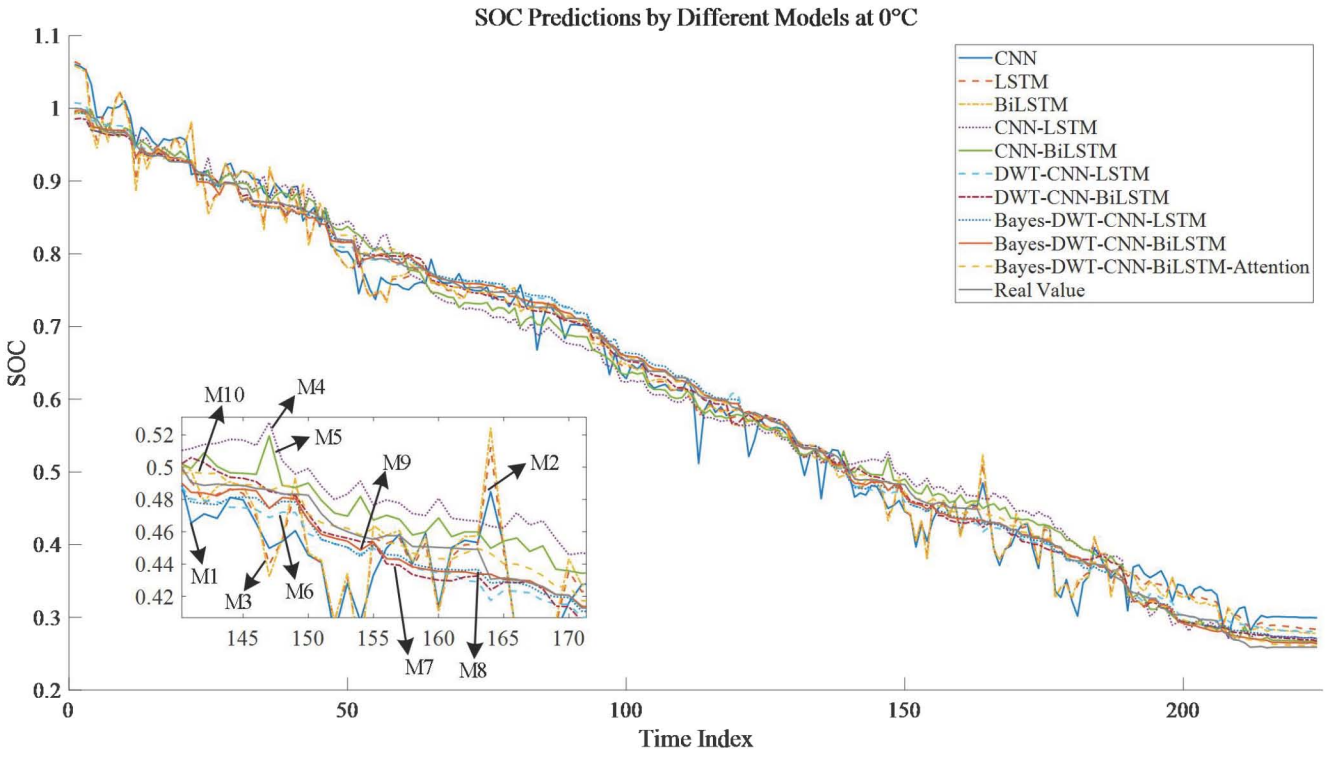

Fig. 12 SOC prediction curves for different models at 0°C.

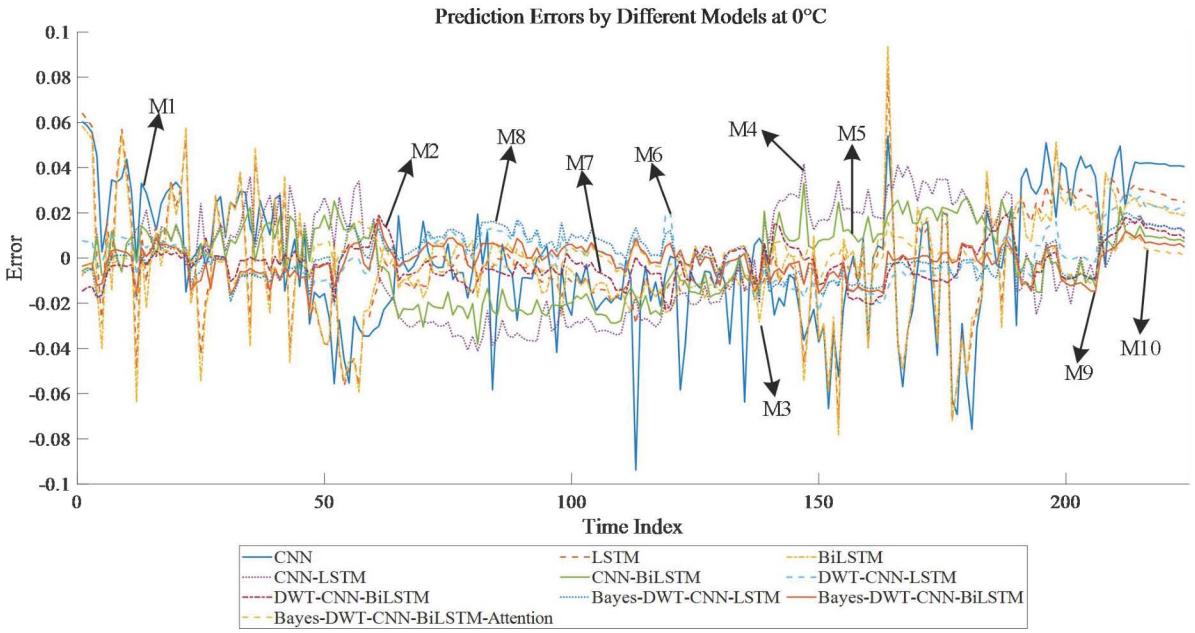

Fig. 13 Predicted error curves for different models at 0°C.

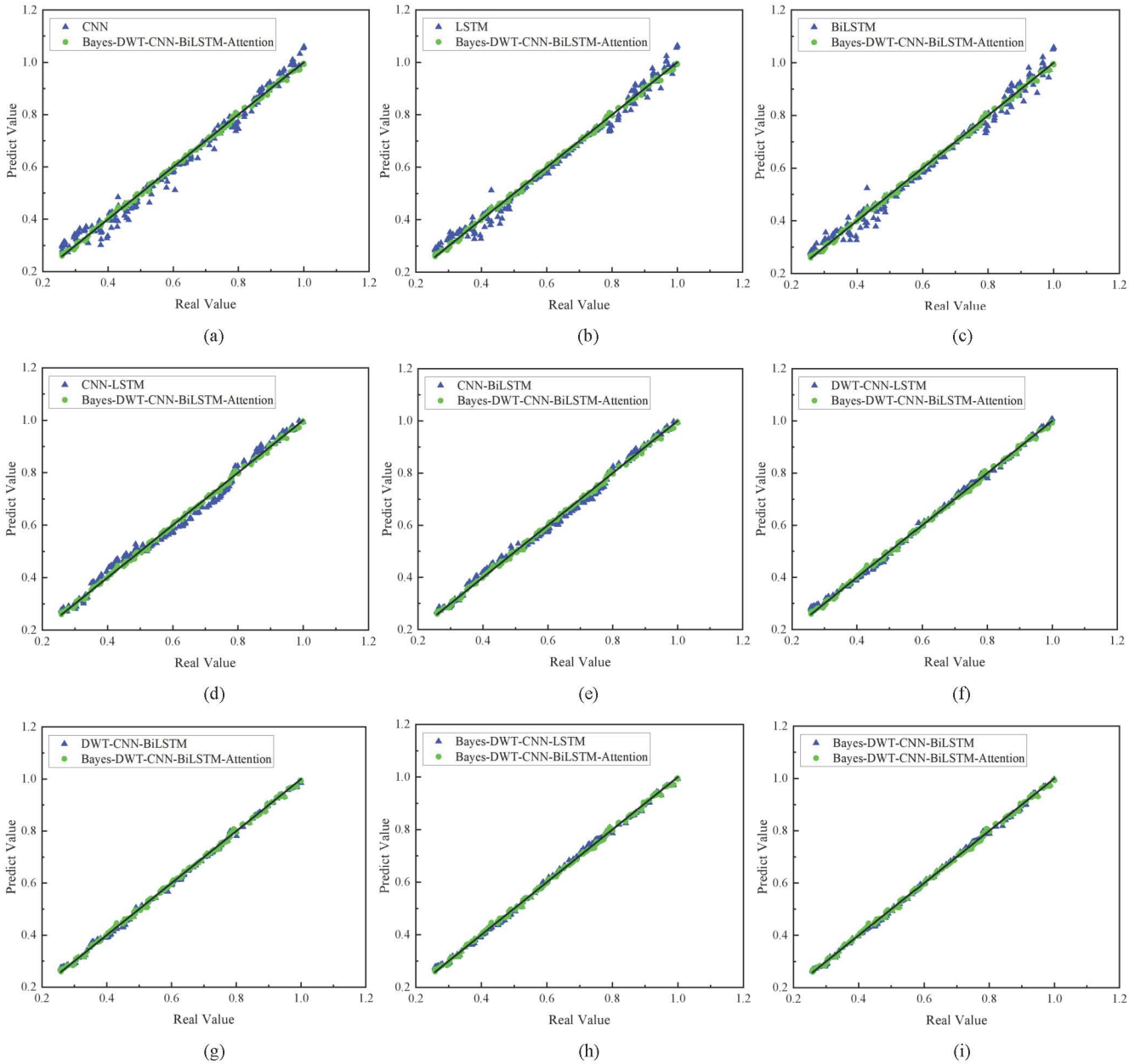

Fig. 14 Scatter plot of different prediction models at 0°C.

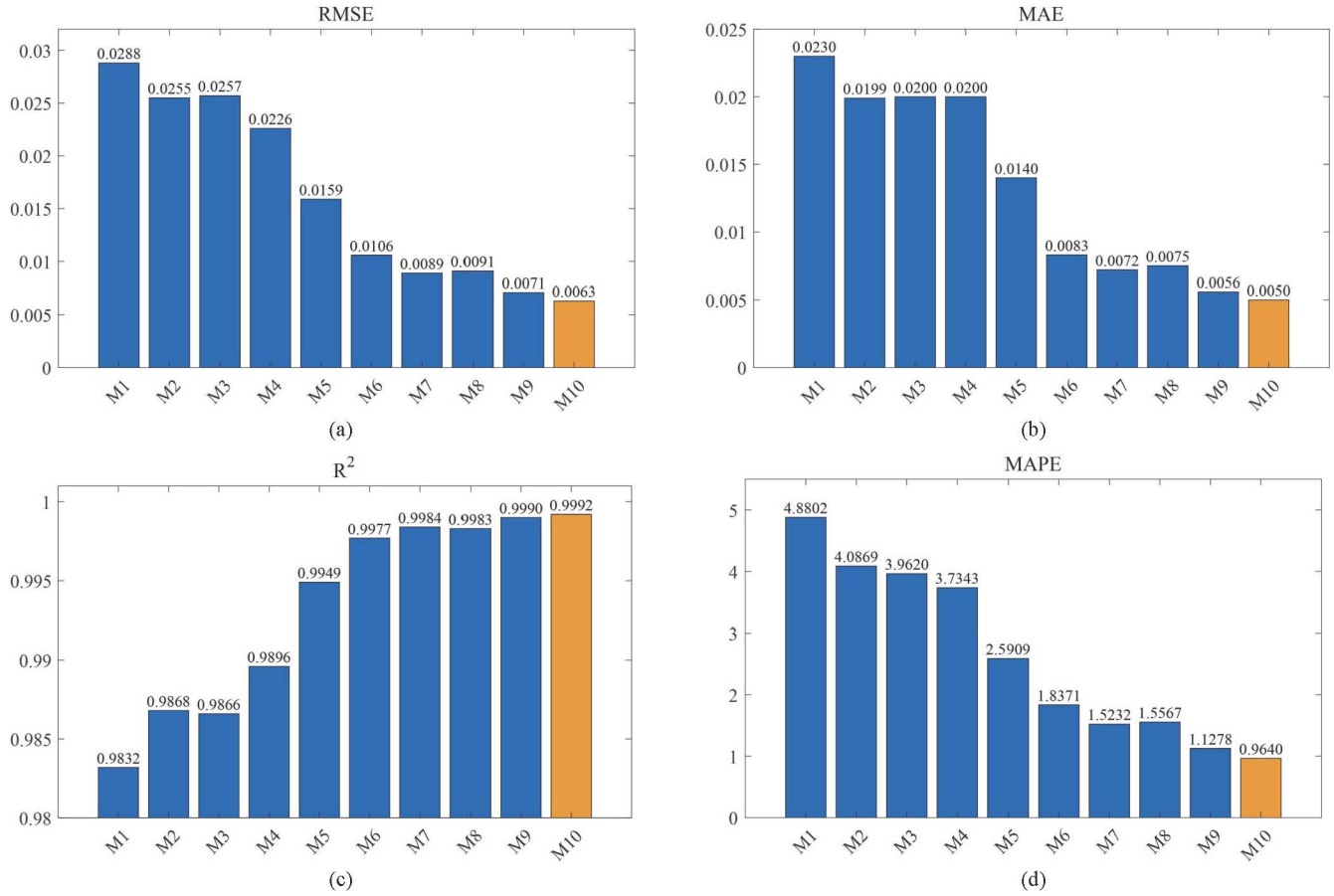

Fig. 15 Bar chart of performance indicators of different prediction models at 0°C.

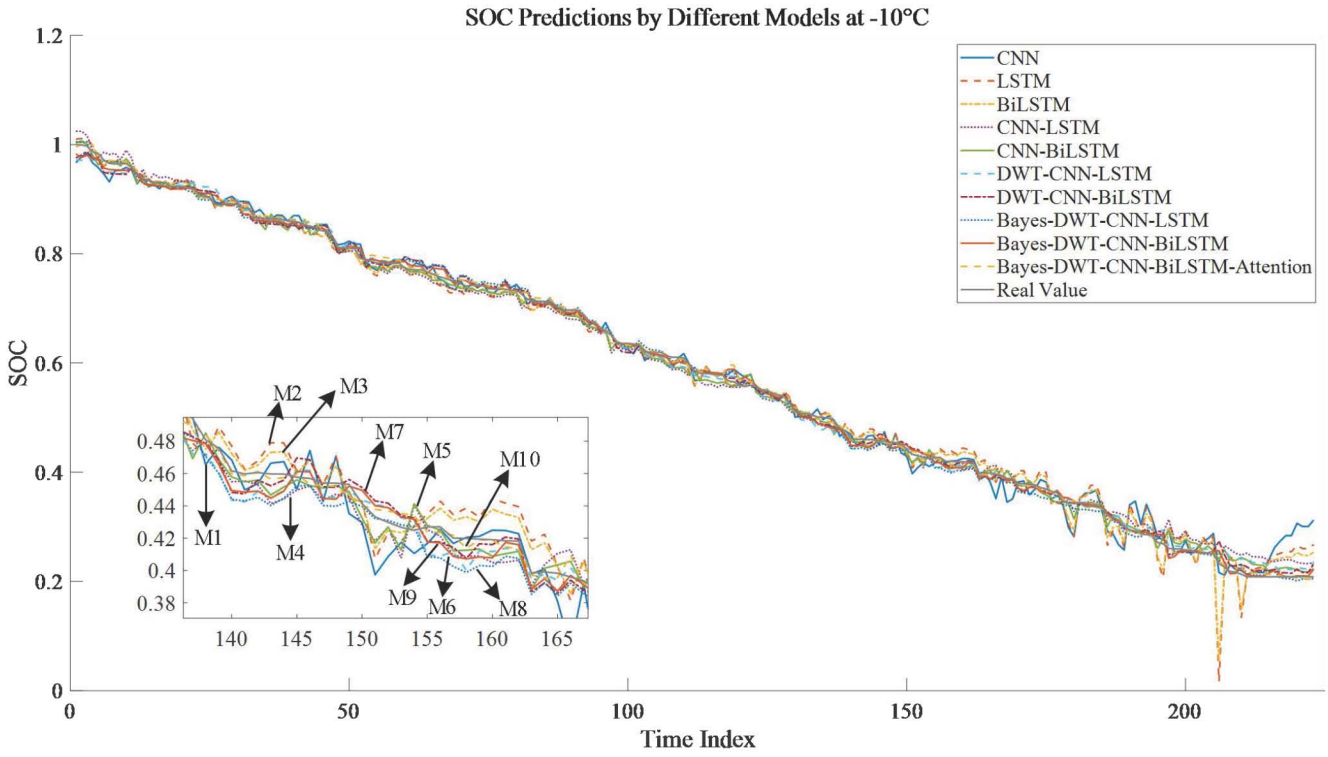

Fig. 16 SOC prediction curves for different models at -10°C.

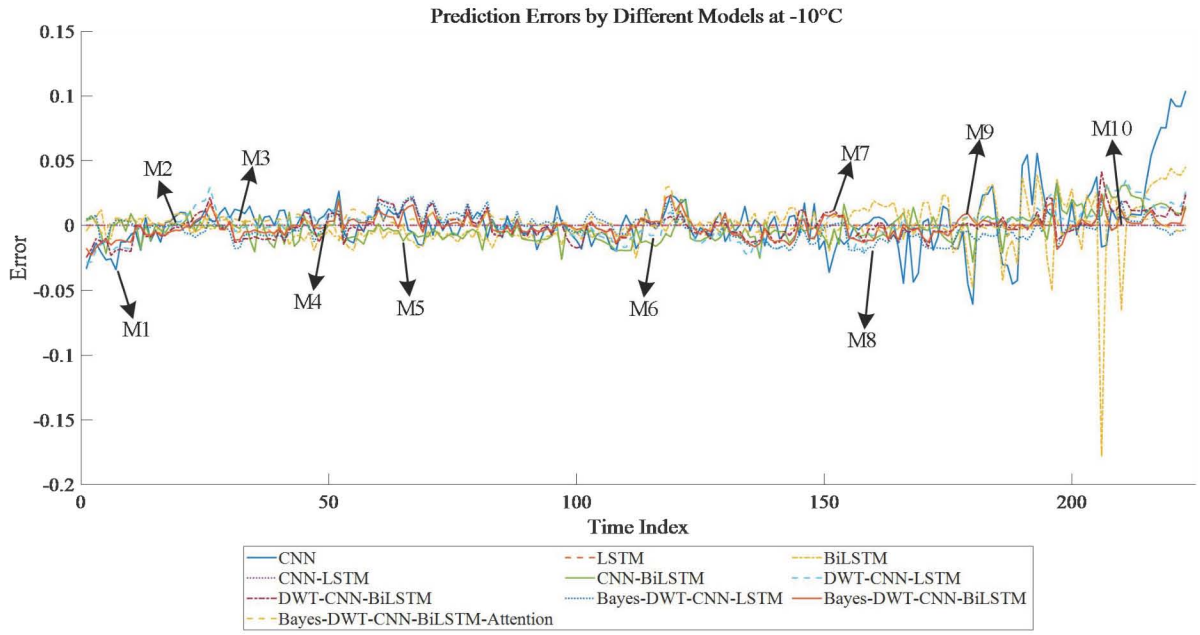

Fig. 17 Predicted error curves for different models at -10°C.

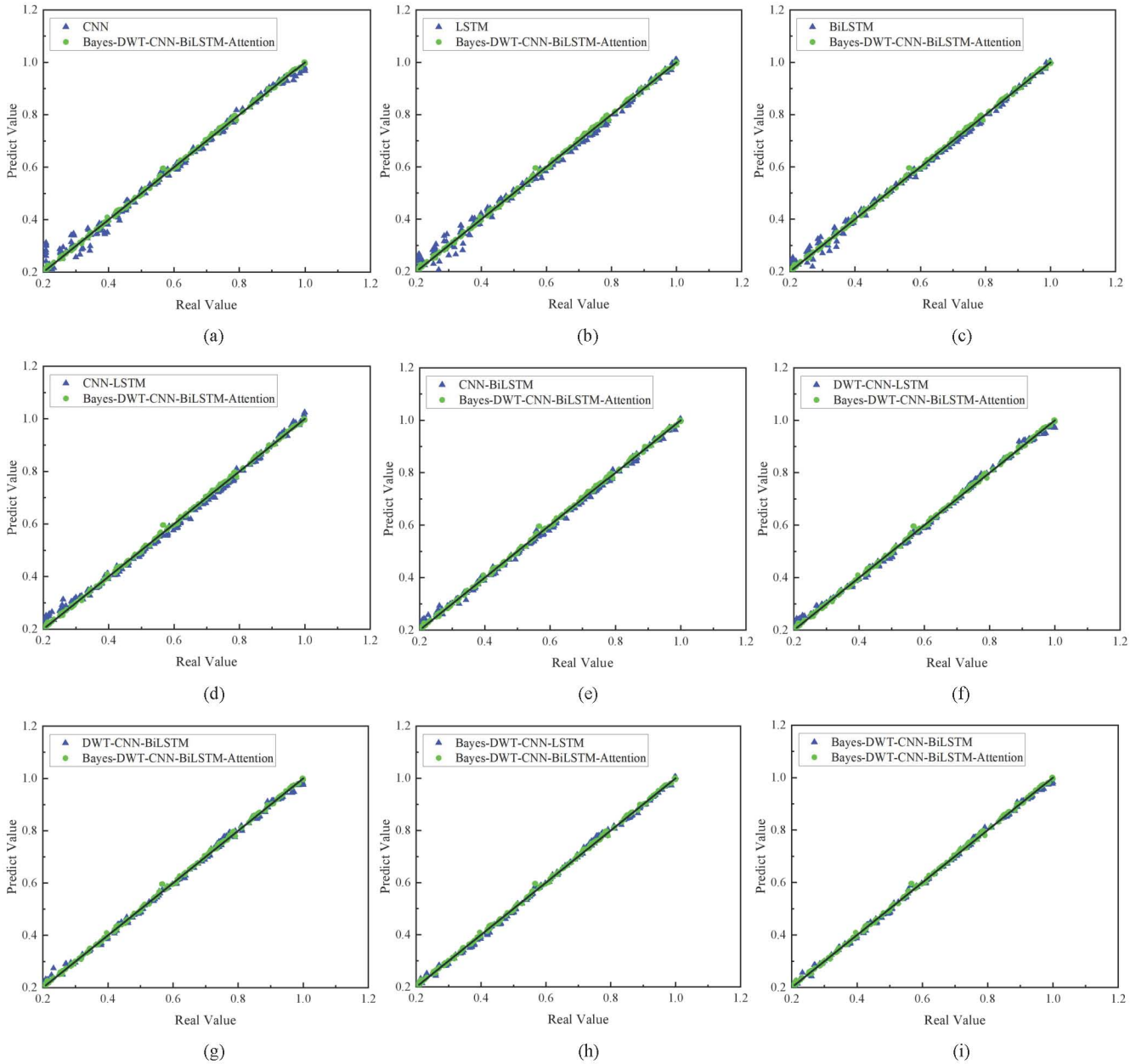

Fig. 18 Scatter plot of different prediction models at -10°C.

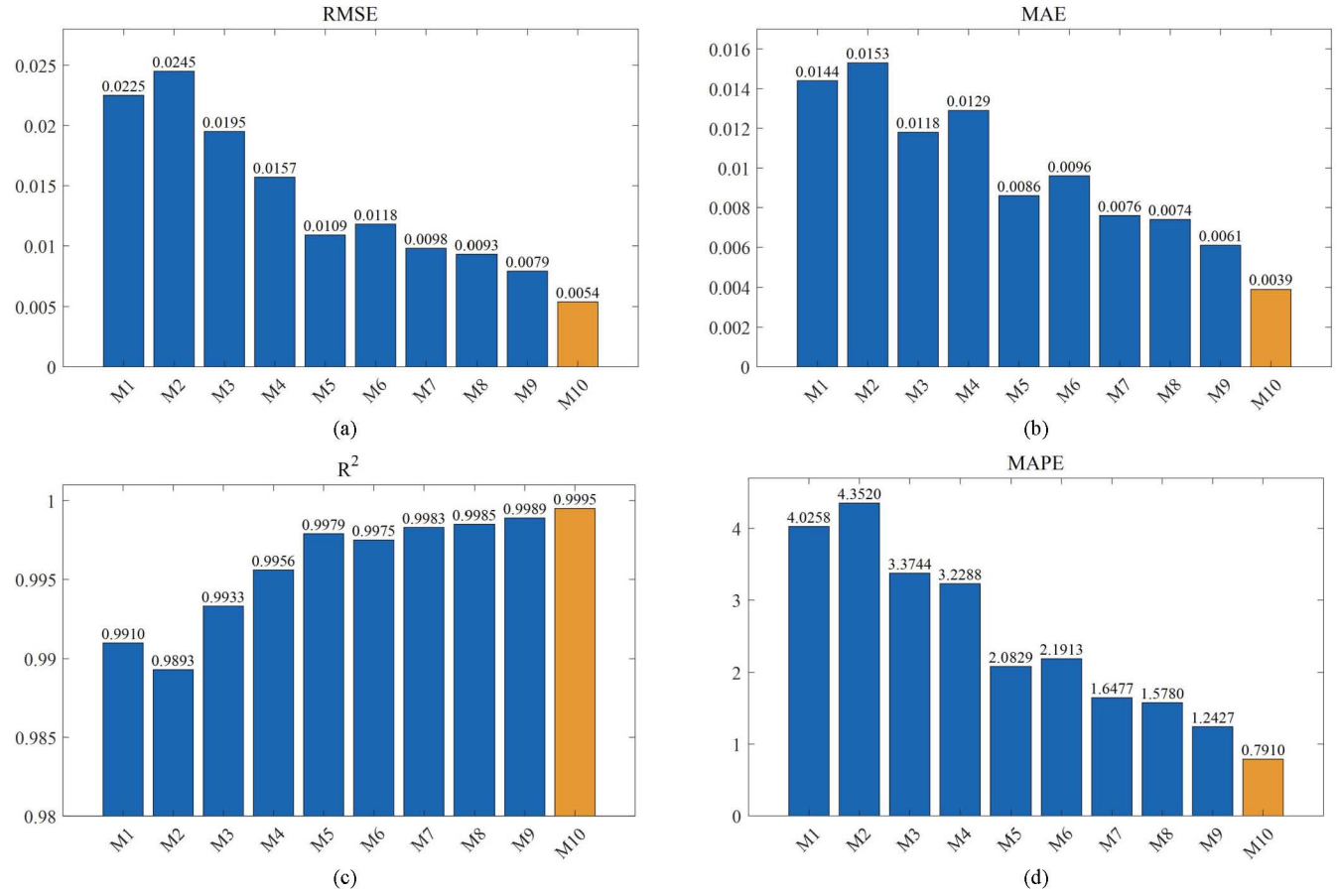

Fig. 19 Bar chart of performance indicators of different prediction models at 10°C.

TABLE II. PERFORMANCE INDICATORS OF DIFFERENT MODELS AT 0°C

	Number	RMSE	MAE	R-squared	MAPE
CNN	M1	0.0288	0.0230	0.9832	4.8802
LSTM	M2	0.0255	0.0199	0.9868	4.0869
BiLSTM	M3	0.0257	0.0200	0.9866	3.9620
CNN-LSTM	M4	0.0226	0.0200	0.9896	3.7343
CNN-BiLSTM	M5	0.0159	0.0140	0.9949	2.5909
DWT-CNN-LSTM	M6	0.0106	0.0083	0.9977	1.8371
DWT-CNN-BiLSTM	M7	0.0089	0.0072	0.9984	1.5232
Bayes-DWT-CNN-LSTM	M8	0.0091	0.0075	0.9983	1.5567
Bayes-DWT-CNN-BiLSTM	M9	0.0071	0.0056	0.9990	1.1278
Bayes-DWT-CNN-BiLSTM-Attention	M10	0.0063	0.0050	0.9992	0.9640

TABLE III. PERFORMANCE INDICATORS OF DIFFERENT MODELS AT -10°C

Model	Number	RMSE	MAE	R-squared	MAPE
CNN	M1	0.0225	0.0144	0.9910	4.0258
LSTM	M2	0.0245	0.0153	0.9893	4.3520
BiLSTM	M3	0.0195	0.0118	0.9933	3.3744
CNN-LSTM	M4	0.0157	0.0129	0.9956	3.2288
CNN-BiLSTM	M5	0.0109	0.0086	0.9979	2.0829
DWT-CNN-LSTM	M6	0.0118	0.0093	0.9975	2.1913
DWT-CNN-BiLSTM	M7	0.0098	0.0076	0.9983	1.6477
Bayes-DWT-CNN-LSTM	M8	0.0093	0.0074	0.9985	1.5780
Bayes-DWT-CNN-BiLSTM	M9	0.0079	0.0061	0.9989	1.2427
Bayes-DWT-CNN-BiLSTM-Attention	M10	0.0054	0.0039	0.9995	0.7910

TABLE IV. PREDICTIVE PERFORMANCE METRICS OF OTHER RESEARCHERS' MODELS ON TURNIGY GRAPHENE 5000MAH 65C LI-ION BATTERY DATA

Model	Reference	Drive Cycle	Temperature	RMSE	MAE	R^2	MAPE
EKF	Ref. [42]	LA92	-10°C	0.0989	N/A	N/A	N/A
			0°C	0.0178	N/A	N/A	N/A
			10°C	0.0101	N/A	N/A	N/A
MAEKF	Ref. [43]	LA92	0°C	0.0089	0.0139	N/A	N/A
			25°C	0.0125	0.0149	N/A	N/A
			40°C	0.0101	0.0129	N/A	N/A
		US06	0°C	0.0300	0.0411	N/A	N/A
			25°C	0.0257	0.0341	N/A	N/A
			40°C	0.0138	0.0322	N/A	N/A
		Mixed	0°C	0.0158	0.0303	N/A	N/A
			25°C	0.0194	0.0325	N/A	N/A
			40°C	0.0143	0.0322	N/A	N/A
ECM	Ref. [44]	LA92	25°C	0.0355	0.0292	N/A	N/A
GASVR	Ref. [45]	LA92	-20°C	0.0195	0.0157	0.9879	N/A
			-10°C	0.0150	0.0130	0.9894	N/A
			0°C	0.0097	0.0097	0.9883	N/A
			10°C	0.0102	0.0084	0.9889	N/A
			25°C	0.0098	0.0084	0.9891	N/A
		NEDC	-20°C	0.0206	0.0163	0.9860	N/A
			-10°C	0.0139	0.0115	0.9850	N/A
			0°C	0.0112	0.0093	0.9877	N/A
			10°C	0.0084	0.0073	0.9892	N/A
			25°C	0.0095	0.0077	0.9892	N/A
Bayes-DWT-CNN-BiLSTM-Attention	Present	LA92	-10°C	0.0054	0.0039	0.9995	0.7910
			0°C	0.0063	0.0050	0.9992	0.9640
			10°C	0.0066	0.0052	0.9991	0.9682

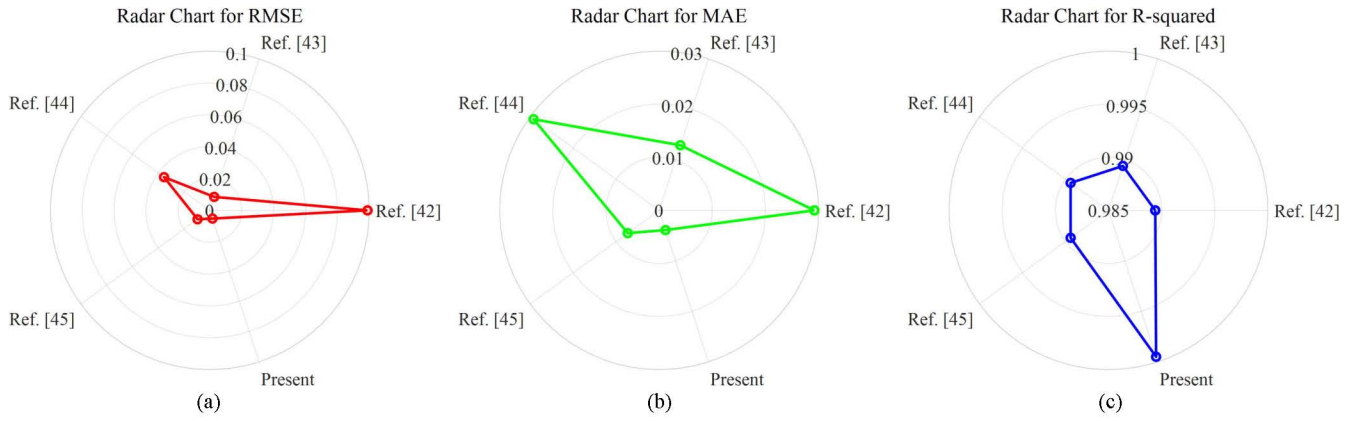

Fig. 20 The radar chart of predicted performance indicators of other researchers on the Turnigy graphene 5000 mAh 65C lithium-ion battery data.

IV. CONCLUSIONS AND PROSPECTS

This paper presents a SE-CNN-BiLSTM state-of-charge (SOC) prediction model for lithium-ion batteries, leveraging Bayesian optimization and wavelet denoising techniques. By employing wavelet transformation to effectively denoise the original dataset, the model significantly mitigates noise interference while preserving essential signal features, thereby enhancing predictive stability. Furthermore, the incorporation of a Squeeze-and-Excitation (SE) module augments the CNN's capacity to allocate weights across diverse features, resulting in more precise feature extraction. Additionally, Bayesian optimization is utilized to fine-tune critical hyperparameters of the BiLSTM architecture, ensuring that the model achieves high predictive accuracy and robust generalization capabilities within complex dynamic environments. Experimental results demonstrate that the proposed SOC prediction model excels under varying temperature conditions and markedly surpasses alternative models in SOC prediction tasks. Simulation outcomes at -10°C, 0°C and 10°C reveal not only significant advantages in performance metrics such as RMSE, MAE and MAPE but also a high R^2 value, validating its superior predictive capability and robustness. In summary, this SE-CNN-BiLSTM framework offers an efficient and reliable solution for SOC prediction in lithium-ion batteries with substantial implications for future battery management system design and optimization.

REFERENCES

[1] J. Carey. "The other benefit of electric vehicles". *Proceedings of the National Academy of Sciences*, vol. 120, no. 3, pp. e2220923120, 2023.

[2] N. Wassiliadis, J. Schneider, A. Frank, L. Wildfeuer, X. Lin, A. Jossen, and M. Lienkamp. "Review of fast charging strategies for lithium-ion battery systems and their applicability for battery electric vehicles". *Journal of Energy Storage*, vol. 44, pp. 103306, 2021.

[3] Z. Cui, L. Wang, Q. Li, and K. Wang. "A comprehensive review on the state of charge estimation for lithium-ion battery based on neural network". *International Journal of Energy Research*, vol. 46, no. 5, pp. 5423-5440, 2022.

[4] K. A. Severson, P. M. Attia, N. Jin, N. Perkins, B. Jiang, Z. Yang, M. H. Chen, M. Aykol, P. K. Herring, D. Fraggedakis, M. Z. Bazant, S. J. Harris, W. C. Harris, W. C. Chueh, and R. D. Braatz. "Data-driven prediction of battery cycle life before capacity degradation". *Nature Energy*, vol. 4, no. 5, pp. 383-391, 2019.

[5] D. N. T. How, M. A. Hannan, M. S. Hossain Lipu, and P. J. Ker. "State of charge estimation for lithium-ion batteries using model-based and data-driven methods: A review". *IEEE Access*, vol. 7, pp. 136116-136136, 2019.

[6] S. Gupta, and A. Gupta. "Dealing with noise problem in machine learning data-sets: A systematic review". *Procedia Computer Science*, vol. 161, pp. 466-474, 2019.

[7] S. Falkner, A. Klein, F. and Hutter. "Practical hyperparameter optimization for deep learning". *International Conference of Learning Representation*, pp. 1-5, 2018.

[8] K. Shankar, Y. Zhang, Y. Liu, L. Wu, and C. H. Chen. "Hyperparameter tuning deep learning for diabetic retinopathy fundus image classification". *IEEE Access*, vol. 8, pp. 118164-118173, 2020.

[9] L. Yang, and A. Shami. "On hyperparameter optimization of machine learning algorithms: Theory and practice". *Neurocomputing*, vol. 415, pp. 295-316, 2020.

[10] J. Peng, J. Luo, H. He, and B. Lu. "An improved state of charge estimation method based on cubature Kalman filter for lithium-ion batteries". *Applied Energy*, vol. 253, pp. 113520, 2019.

[11] C. Chen, R. Xiong, R. Yang, W. Shen, and F. Sun. "State-of-charge estimation of lithium-ion battery using an improved neural network model and extended Kalman filter". *Journal of Cleaner Production*, vol. 234, pp. 1153-1164, 2019.

[12] C. Li, F. Xiao, and Y. Fan. "An approach to state of charge estimation of lithium-ion batteries based on recurrent neural networks with gated recurrent unit". *Energies*, vol. 12, no. 9, pp. 1592, 2019.

[13] F. Yang, S. Zhang, W. Li, and Q. Miao. "State-of-charge estimation of lithium-ion batteries using LSTM and UKF". *Energy*, vol. 201, pp. 117664, 2020.

[14] Y. Tian, R. Lai, X. Li, L. Xiang, and J. Tian. "A combined method for state-of-charge estimation for lithium-ion batteries using a long short-term memory network and an adaptive cubature Kalman filter". *Applied Energy*, vol. 265, pp. 114789, 2020.

[15] C. Bian, H. He, S. Yang, and T. Huang. "State-of-charge sequence estimation of lithium-ion battery based on bidirectional long short-term memory encoder-decoder architecture". *Journal of Power Sources*, vol. 449, pp. 227558, 2020.

[16] X. Ren, S. Liu, X. Yu, and X. Dong. "A method for state-of-charge estimation of lithium-ion batteries based on PSO-LSTM". *Energy*, vol. 234, pp. 121236, 2021.

[17] Y. Liu, J. Li, G. Zhang, B. Hua, and N. Xiong. "State of charge estimation of lithium-ion batteries based on temporal convolutional network and transfer learning". *IEEE Access*, vol. 9, pp. 34177-34187, 2021.

[18] J. Chen, X. Feng, L. Jiang, and Q. Zhu. "State of charge estimation of lithium-ion battery using denoising autoencoder and gated recurrent unit recurrent neural network". *Energy*, vol. 227, pp. 120451, 2021.

[19] K. Yang, Y. Tang, S. Zhang, and Z. Zhang. "A deep learning approach to state of charge estimation of lithium-ion batteries based on dual-stage attention mechanism". *Energy*, vol. 244, pp. 123233, 2022.

[20] S. Sun, J. Sun, Z. Wang, Z. Zhou, and W. Cai. "Prediction of battery SOH by CNN-BiLSTM network fused with attention mechanism". *Energies*, vol. 15, no. 12, pp. 4428, 2022.

[21] Z. Cui, L. Kang, L. Li, L. Wang, and K. Wang. "A hybrid neural network model with improved input for state of charge estimation of lithium-ion battery at low temperatures". *Renewable Energy*, vol. 198, pp. 1328-1340, 2022.

[22] W. Wang, B. Ma, X. Hua, B. Zou, L. Zhang, H. Yu, K. Yang, S. Yang, and X. Liu. "End-cloud collaboration approach for state-of-charge estimation in lithium batteries using CNN-LSTM and UKF". *Batteries*, vol. 9, no. 2, pp. 114, 2023.

[23] B. Yan, W. Zheng, D. Tang, Y. LaiLi, and Y. Xing. "A knowledge-constrained CNN-BiLSTM model for lithium-ion batteries state-of-charge estimation". *Microelectronics Reliability*, vol. 150, pp. 115112, 2023.

[24] H. Xu, L. Wu, S. Xiong, W. Li, A. Garg, and L. Gao. "An improved CNN-LSTM model-based state-of-health estimation approach for lithium-ion batteries". *Energy*, vol. 276, pp. 127585, 2023.

[25] C. Rincón-Maya, F. Guevara-Carazas, F. Hernández-Barajas, C. Patiño-Rodríguez, and O. Usuga-Manco. "Remaining useful life prediction of lithium-ion battery using ICC-CNN-LSTM methodology". *Energies*, vol. 16, no. 20, pp. 7081, 2023.

[26] M. Li, C. Li, Q. Zhang, W. Liao, and Z. Rao. "State of charge estimation of Li-ion batteries based on deep learning methods and particle-swarm-optimized Kalman filter". *Journal of Energy Storage*, vol. 64, pp. 107191, 2023.

[27] H. Yu, L. Zhang, W. Wang, S. Li, S. Chen, S. Yang, J. Li, and X. Liu. "State of charge estimation method by using a simplified electrochemical model in deep learning framework for lithium-ion batteries". *Energy*, vol. 278, pp. 127846, 2023.

[28] Z. Sherkatghanad, A. Ghazanfari, and V. Makarenkov. "A self-attention-based CNN-Bi-LSTM model for accurate state-of-charge estimation of lithium-ion batteries". *Journal of Energy Storage*, vol. 88, pp. 111524, 2024.

[29] C. Lin, X. Tuo, L. Wu, G. Zhang, and X. Zeng. "Accurate capacity prediction and evaluation with advanced SSA-CNN-BiLSTM framework for lithium-ion batteries". *Batteries*, vol. 10, no. 3, pp. 71, 2024.

[30] A. Halidou, Y. Mohamadou, A. A. A. Ari, and E. J. G. Zacko. "Review of wavelet denoising algorithms". *Multimedia Tools and Applications*, vol. 82, no. 27, pp. 41539-41569, 2023.

[31] J. Kim, H. M. Hasanien, and R. K. Tagayi. "Investigation of noise suppression in experimental multi-cell battery string voltage applying various mother wavelets and decomposition levels in discrete wavelet transform for precise state-of-charge estimation". *Journal of Energy Storage*, vol. 73, pp. 109196, 2023.

[32] P. Kollmeyer, and M. Skells. "Turnigy graphene 5000mAh 65C li-ion battery data". *Mendeley Data*, vol. 1, pp. 10-17632, 2020.

[33] O. M. Katipoğlu. "Combining discrete wavelet decomposition with soft computing techniques to predict monthly evapotranspiration in semi-arid Hakkâri province, Türkiye". *Environmental Science and Pollution Research*, vol. 30, no. 15, pp. 44043-44066, 2023.

[34] A. Abdallah, B. Bengherbia, P. Wira, and N. Alaoui. "The effectiveness of optimal discrete wavelet transform parameters obtained using the genetic algorithm for ECG signal denoising". *Revue d'Intelligence Artificielle*, vol. 37, no. 6, 2023.

[35] A. W. Salehi, S. Khan, G. Gupta, B. I. Alabduallah, A. Almjaly, H. Alsolai, T. Siddiqui, and A. Mellit. "A study of CNN and transfer learning in medical imaging: Advantages, challenges, future scope". *Sustainability*, vol. 15, no. 7, pp. 5930, 2023.

[36] X. Jin, Y. Xie, X. S. Wei, B. R. Zhao, Z. M. Chen, and X. Tan. "Delving deep into spatial pooling for squeeze-and-excitation networks". *Pattern Recognition*, vol. 121, pp. 108159, 2022.

[37] J. Ai, S. Hou, M. Wu, B. Chen, and H. Yan. "MPGSE-D-LinkNet: multiple-parameters-guided squeeze-and-excitation integrated D-LinkNet for road extraction in remote sensing imagery". *IEEE Geoscience and Remote Sensing Letters*, 2023.

[38] P. Hu, W. F. Tang, C. H. Li, S. L. Mak, C. Y. Li, and C. C. Lee. "Joint state of charge (SOC) and state of health (SOH) estimation for lithium-ion batteries packs of electric vehicles based on NSSR-LSTM neural network". *Energies*, vol. 16, no. 14, pp. 5313, 2023.

[39] P. Singla, M. Duhan, and S. Saroha. "An ensemble method to forecast 24-h ahead solar irradiance using wavelet decomposition and BiLSTM deep learning network". *Earth Science Informatics*, vol. 15, no. 1, pp. 291-306, 2022.

[40] B. Alizadeh, A. G. Bafti, H. Kamangir, Y. Zhang, D. B. Wright, and K. J. Franz. "A novel attention-based LSTM cell post-processor coupled with bayesian optimization for streamflow prediction". *Journal of Hydrology*, vol. 601, pp. 126526, 2021.

[41] E. T. Habtemariam, K. Kekeba, M. Martínez-Ballesteros, and F. Martínez-Álvarez. "A Bayesian optimization-based LSTM model for wind power forecasting in the Adama district, Ethiopia". *Energies*, vol. 16, no. 5, pp. 2317, 2023.

[42] F. Khanum, E. Louback, F. Duperly, C. Jenkins, P. J. Kollmeyer, and A. Emadi. "A Kalman filter based battery state of charge estimation MATLAB function". *2021 IEEE Transportation Electrification Conference & Expo (ITEC)*, pp. 484-489, 2021.

[43] S. Rout, and S. Das. "A robust modified adaptive extended Kalman filter for state-of-charge estimation of rechargeable battery under dynamic operating condition". *Electrical Engineering*, 2024.

[44] T. Hawsawi, M. Alolaiwy, Y. Taleb, A. Mezaael, and M. Zohdy. "An improved thevenin model-based state-of-charge estimation of a commercial lithium-ion battery using Kalman filter". *2023 IEEE Smart World Congress (SWC)*, pp. 735-741, 2023.

[45] C. Chen, Z. Li, and J. Wei. "Estimation of lithium-ion battery state of charge based on genetic algorithm support vector regression under multiple temperatures". *Electronics*, vol. 12, no. 21, pp. 4433, 2023.